Digital Comprehensive Summaries of Uppsala Dissertations
from the Faculty of Science and Technology 2272

Fundamentals and applications of microplasma sources

Actuating, Sensing, and Nonlinearly Approximating.

RAGNAR SETON

ACTA UNIVERSITATIS
UPSALIENSIS
2023

ISSN 1651-6214
ISBN 978-91-513-1819-6
urn:nbn:se:uu:diva-500778

UPPSALA
UNIVERSITET

Dissertation presented at Uppsala University to be publicly examined in Polhemsalen, 10134, Ångströmlaboratoriet, Lägerhyddsvägen 1, Uppsala, Wednesday, 14 June 2023 at 09:00 for the degree of Doctor of Philosophy. The examination will be conducted in English. Faculty examiner: Associate Professor Donatella Puglisi (Linköping University, Department of Physics, Chemistry and Biology).

Abstract
Seton, R. 2023. Fundamentals and applications of microplasma sources. Actuating, Sensing, and Nonlinearly Approximating.. *Digital Comprehensive Summaries of Uppsala Dissertations from the Faculty of Science and Technology* 2272. 54 pp. Uppsala: Acta Universitatis Upsaliensis. ISBN 978-91-513-1819-6.

The research presented in this thesis covers a wide range of applications for, and integrations of, a stripline split-ring resonator (SSRR) microplasma source. Common throughout the presented works is the always present, but sometimes secondary, focus on analyzing the light and matter that is emitted as gas is flowed through theplasma of the SSRR.

When evaluated as a heater in a cold-gas microthruster intended for attitude adjustment and orbit maintenance of miniaturized satellites, the plasma was shown to be a more efficient than two modes of resistive heating in improving the specific impulse of the thruster. Furthermore, the ionized exhaust plume of the thruster was used to derive a novel method of estimating its efficiency. In further analysis of the plasma parameters, correlations between supplied power, ion density, and thrust efficiency were uncovered and verified by Langmuir probe measurements.

In subsequent experiments, the use of the SSRR as a residual gas analyzer was explored, first by comparing different classes of regression methods for determining gas species concentrations from emitted UV-NIR spectra from the plasma. In a second study, the wide range spectrometer was replaced with an optical filter and a photodetector, in a differential gas sensor setup where the regression methods were replaced with peak intensity differentiation.

With the SSRR's prospects as a gas sensor confirmed, further work focused on integrating it in a transcutaneous blood gas monitoring (TBM) system. To address the shortcomings of existing systems, a series of three studies covered the fabrication and evaluation of *(i)* A soft gas-collecting patch that, with its accompanying microfluidics, transported the gas that permeates the skin to the sensor, *(ii)* A novel fabrication technique to integrate an electrical interface in the bulk of the patch, and a prototype out-of-plane skin heater, and *(iii)* A theoretical model that related the transcutaneous gas composition to blood gas concentration based on a computational fluid dynamics model. Finally, the sensor and gas collector were integrated in a fully functional TBM system.

In conclusion, the thesis explores the use of an SSRR throughout the three cornerstone configurations of microsystem technology: as an *actuator* for microsatellite propulsion, as a *sensor* for gas measurements, and integrated in a *system* for blood gas monitoring.

Keywords: Stripline Split-ring Resonator, Microplasma, Optical Emission Spectroscopy, Medical Technology, Transcutaneous Blood Gas Monitoring, Small Satellites, Microthruster, Cold Gas Thruster

Ragnar Seton, Department of Materials Science and Engineering, Microsystems Technology, Box 35, Uppsala University, SE-751 03 Uppsala, Sweden.

ISSN 1651-6214
ISBN 978-91-513-1819-6
URN urn:nbn:se:uu:diva-500778 (http://urn.kb.se/resolve?urn=urn:nbn:se:uu:diva-500778)

Dedicated to all the tax payers that make independent research possible.

List of papers

This thesis is based on the following papers, which are referred to in the text by their Roman numerals.

I P. Sturesson, **R. Seton**, L. Klintberg, G. Thornell, A. Persson. *Effect of Resistive and Plasma Heating on the Specific Impulse of a Ceramic Cold Gas Thruster*, IEEE Journal of Microelectromechanical Systems, Vol. 28, No. 2, April 2019

II **R. Seton**, P. Sturesson, A. Persson. *Investigating the plasma properties of a Xe-microplasma thruster*, IOP Conf. Series: Journal of Physics: Conf. Series **1319** (2019) 012013

III **R. Seton**, G. Thornell, A. Persson. *Compliance of a microstructured, soft sampling device for transcutaneous blood gas monitoring*, RSC Advances, 2020, **10**, 36386

IV **R. Seton**, Z. Khaji, A. Persson. *PDMS-Polyimide transcutaneous blood gas collector with self-folding out-of-plane heater elements*, IOP Journal of Micromechanics and Microengineering **33** (2023) 065006 (11pp)

V **R. Seton**, A. Persson. *A structured evaluation of regression models for predicting CO_2 concentration from plasma emission spectra*, Spectrochimica Acta Part B: Atomic Spectroscopy 194 (2022) 106467

VI A. Persson, **R. Seton**. *Modeling and evaluation of a rate-based transcutaneous blood gas monitor*, IEEE Transactions on Biomedical Engineering, Submitted, Under review

VII **R. Seton**, M. Berglund, A. Persson. *Differential spectrometric gas sensor with dual out-of-phase microplasma sources*, Applied Physics Letters, Submitted

Summary of Contributions

The Roman numerals correspond to the numbers in the list of papers.

I Part of concept, part of planning, part of experimental work and analysis, part of writing.

II Most of concept, planning, experimental work and analysis, and writing.

III Most of concept, planning, experimental work and analysis, and writing.

IV Major part of concept, most of planning, experimental work and analysis, and writing.

V Most of concept, planning, experimental work and analysis, and writing.

VI Major part of concept and planning, most of experimental work and analysis, part of writing.

VII Part of concept and planning, major part of experimental work and analysis, and part of writing.

Related Work

Additional Publications

R1 T. Ribeiro, A. D'Ambrosio, G. J. Domínguez Calabuig, D. Athanasopoulos, H. Bates, C. Riegler, O. Gassot, S. Gerig, J. L. Gómez-González, N. Huber, **R. Seton**, T. E. C. Magalhães. *CARINA: A sample return mission concept to a near-Earth D-type asteroid*, submitted manuscript under review at Acta Astronautica

Datasets

D1 **R. Seton**, Z. Khaji, A. Persson. *PDMS-Polyimide transcutaneous blood gas collector with self-folding out-of-plane heater elements, dataset* (1.0.0), Zenodo, `https://doi.org/10.5281/zenodo.7414413`

D2 **R. Seton**, A. Persson. *A structured evaluation of regression models for predicting CO_2 concentration from plasma emission spectra, dataset* (1.0.0), Zenodo, `https://doi.org/10.5281/zenodo.7860727`

Code

C1 **R. Seton**. *åstcCCS*, MATLAB class to handle Thorlabs CCS series spectrometers. `https://gitlab.com/ragnarseton/astcCCS`

C2 **R. Seton**, *Zygo viewer*, MATLAB viewer for datx-files produced by optical profilers from Zygo. `https://gitlab.com/ragnarseton/view_zygo`

C3 **R. Seton**, *FLIR viewer*, MATLAB class to handle thermal images and videos from FLIR thermal cameras. `https://gitlab.com/ragnarseton/flir_exif`

Contents

1 Introduction 11
1.1 Outline and Objectives 11
1.2 Microsystems Technology 12
1.3 SSRR Microplasma Sources 13

2 Sensors 15
2.1 Regression Analysis of Spectral Data 20
2.1.1 An experimental design for method comparison 23
2.1.2 Evaluating regression models as sensors 25
2.1.3 Out of domain predictions 28
2.2 Single peak differential gas sensor 29

3 Systems 32
3.1 Transcutaneous Blood Gas Monitoring 32
3.2 Micropatterning PDMS 34
3.3 Electrical Interfaces & Blood Gas Concentration 35

4 Actuators 39
4.1 Plasma heated cold gas microthrusters 40
4.1.1 Plasma properties and thruster efficiency 42

5 Concluding Remarks and Future Work 43

6 Acknowledgements 45

7 Svensk sammanfattning 47

Bibliography 50

Abbreviations

CCD	Charge-Coupled Device
CMOS	Complementary Metal-Oxide-Semiconductor
EM	Electromagnetic
FWC	Full Well Capacity
GLONASS	Global Navigation Satellite System
GPS	Global Positioning System
ISO	International Organization for Standardization
LEO	Low Earth Orbit
MSE	Mean Squared Error
MST	Microsystems Technology
NN	Neural Network
PCC	Pearson's Correlation Coefficient
PDMS	Polydimethylsiloxane
PLS	Partial Least Squares *or* Projection to Latent Structures
QE	Quantum Efficiency
SNR	Signal-to-Noise Ratio
SNV	Standard Normal Variate
SSRR	Stripline Split-Ring Resonator
TBM	Transcutaneous Blood gas Monitoring
TCM	Transcutaneous Monitoring
WHO	World Health Organization

1. Introduction

Let there be light, and there was plasma. While this is not the famous quote popularized by various religious scripts, it could have been – had they only been more concerned with reality. Because it is massive bodies of plasma that provide us, and the rest of the universe, with the light that is the prerequisite for life as we know it. This light not only grants us life, but knowledge as well. It tells us the story of the universe, of its history and creation, and which atoms and molecules exist in places so far away that by the time we see their traces, they are long gone.

It should be noted that I am taking some artistic liberties with the phrase *tell us* above – a regular conversation would be quite cumbersome if it required spectral analysis to understand what the other person is saying. The point is that it is possible to determine the composition of mindbogglingly distant matter from only the light it emits. The same goes for matter here on Earth. Here, however, plasma is a little less common than in space. We see it in auroras, lightning, and funky looking lamps, but outside of a brief period in the mid -00s, when plasma displays were all the rage, it is rarely thought of as useful in daily life. This is where the research performed for this thesis comes in. Here, I will present the findings attained from using a microplasma source as an actuator, sensor, and figurative star of a complete microsystem.

1.1 Outline and Objectives

The thesis is divided into three sections, each centered around one specific configuration of microsystems technology (MST); sensors, actuators, and fully integrated systems. Each section provides an introduction to the subject matter within which the corresponding publications, listed in the *List of papers* above, have been authored, and tries to provide a balanced summary of their contribution to the respective field or application. The papers and their results are thus discussed as an extension to the introduction and review of each subject.These aim to provide the context needed to understand the challenges addressed in the publications, and the novelty they provide, rather than being an exhaustive review of their individual fields.

The primary target audience of the thesis is undergraduate students and enthusiasts of science, technology, and engineering, but my hope is that both more and less veteran readers will also enjoy the read. With that in mind, we will start with an introduction to MST in general and the stripline split ring resonator (SSRR) microplasma sources I have been using in my research, in particular.

1.2 Microsystems Technology

As indicated by the name, MST refers to systems whose defining features are in the micrometer (μm), or *micron*, or millionths of a meter, range. To put this into perspective, if we were to scale up a μm to be the length of a regular 33 cl (~11 oz) soda can, the correspondingly scaled up can would reach outer space.

While there are plenty of things in our daily lives that have one or two dimensions in this size range, the tape of a compact cassette (a timely reference) and fine spider webs for example, things that are no bigger than a few μm in any direction can not be seen with the naked eye. This, to a certain degree, translates to fabrication as well – if you have ever sharpened a knife to the point where you can let if fall through a tomato, you have created a microstructure! Thus, it is as doable in one dimension as it is complex in two or three.

The fact that MST covers a range of components that can be anything from barely submillimeter down to easily submicron makes the term *microfabrication* encompass an equally wide range of techniques. The processes that historically are most likely to come to mind when talking about microfabrication are cleanroom-based ones, such as photolithography and wet and dry etching [1]. As any MST thesis would be incomplete without a short introduction to these techniques, here follows my due diligence. Photolithography is a process that involves coating a substrate with a thin film of a light-sensitive polymer called photoresist, transferring a geometric design onto it with what is usually very short wavelength light shone through a pre-made mask (think extremely high resolution shadow puppets), washing off the sections that did not get cross-linked, and then pouring over more chemicals to etch away the bits of the underlying substrate that were uncovered. By repeating this process, it is possible to produce small, complex structures. The reason for this technique being such a staple of MST is its compatibility with the staple material – silicon – and its scalability, both up and down. Down with respect to resolution, with the latest commercial applications of it reaching single digit nanometer resolutions, and up with respect to numbers, as it is the technique that has produced the most units of any single component in the history of humanity[1]. And while this will be the last you read about this particular technique in this thesis, we will get back to the concept of how fabrication processes scale in **Paper IV**. That is because scalability, together with the ability to rapidly prototype new designs and provide high resolution results are the three primary features a researcher is generally interested in, but can unfortunately usually only pick two of. The choice of fabrication method has thus, at least historically, been governed by two things, the lowest resolution required by the application, and how much money the researcher in question has access to. With recent advancements in low cost, high resolution fabrication methods [2], the latter bar is, fortunately, being pushed downward. The former is what makes comparatively low-tech

[1]Reportedly, over 10^{21} transistors have been produced, which similar in magnitude to a back-of-the-envelope approximation of the number of stars in the universe.

fabrication methods, such as screen printing [3], milling [4], and laser cutting ubiquitous in MST research (and part of this thesis). Additionally, additive manufacturing in general, and microscale 3D-printing in particular, have seen rapid growth over the last decade and are already the microfabrication methods of choice in many biomedical applications [5].

Concludingly, there have been works written solely about the fabrication techniques in MST that make the earlier mentioned religious texts seem like pamphlets by comparison. Even the one I used to reference photolithography above, [1], is a three volume, 2000 page behemoth. So, instead of naming more techniques and just adding references, let us move on to the microsystem this thesis is centered around.

1.3 SSRR Microplasma Sources

When not abbreviated, stripline split-ring resonators are quite the mouthful. Before getting into the microplasma part of it, we will use figure 1.1 to break down its terms. *Stripline* simply refers to where in the dielectric a conductive strip is located. Figure 1.1a compares a stripline (right), where the gold-colored conductor (or waveguide in our context) is located inside the dielectric with ground planes enclosing it, with a microstrip (left), where it lies on top. In the next subfigure, 1.1b, we see the *Split-Ring Resonator*, a conductive strip that is essentially a curved antenna forming a ring with a small gap between its ends. While the design considerations and governing physics of the resonator itself are quite interesting in their own right, I will defer to the original publications [6, 7] for the details. The long and short of it is that the circumference of the split-ring is exactly half a wavelength of the radio frequency power coming out of the power supply driving it. This ensures that the voltage across the cavity in the ring is maximized. Additionally, the length, width, and angular offset of the strip connecting the ring to the power supply is adjusted to minimize the amount of power reflected by the ring, a design process called impedance matching. As a final note on the design of the SSRR, we return to the first S. The stripline design addresses an issue plaguing microstrip SRRs where changes in the surrounding relative permittivity affect the resonance frequency of it. This means that touching the split-ring, or even significant changes in the ambient humidity, would affect its plasma properties – or even kill it entirely. Another aspect of it is tied to the resonance frequency of the SSRR we used, 2.4 GHz. This frequency undoubtedly rings a bell to users of Wi-Fi routers, wireless keyboards and mice, or microwave ovens, as it is the same one as many of those appliances operate in, and the SRR is thus susceptible to interference from them. Adding the encapsulating groundplanes, however, removes the interference [6]. This self-imposed need for added shielding might seem cost-ineffective, but with the prevalence of all of these other antennas operating at the same frequency comes the benefit of cheap, readily

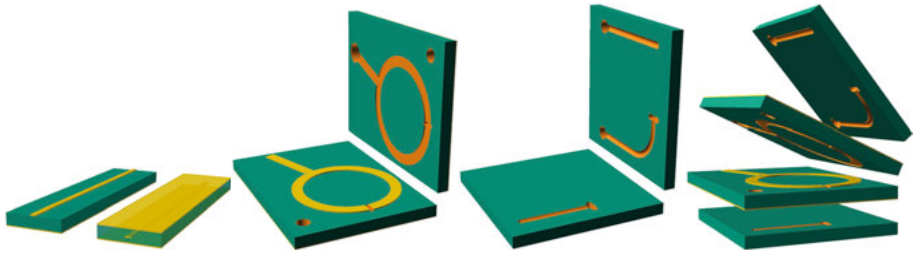

(a) Microstrip vs. Stripline. *(b)* Split-ring resonator sandwich. *(c)* Fluidics to guide gas samples through the plasma. *(d)* Microplasma source with with fluidics-attachment.

Figure 1.1. Starting with a comparison of microstrip and stripline waveguides in *(a)*, the following figures shows the different components of the microplasma source.

available driving components. Granted, the requirements of the power supply for the resonator in the microplasma source differs a bit from that of a Wi-Fi antenna in a laptop, but being able to utilize a mature supply chain for parts of it ensures the availability of spare parts and that the serviceability, and thus longevity, of a power supply is not tied to one single manufacturer.

In papers **I** and **II**, the microplasma source only included the elements seen in figure 1.1b. In the subsequent five papers, however, the fluidics shown in figure 1.1c were integrated to facilitate flowing gas through the plasma. It is the same design as described in reference [8], sans the laser.

Finally it should be noted that while this design offers a stable, dense, cold plasma that can be operated at relatively high pressures, none of the results in the papers are intrinsically tied to it. It should be entirely possible to reproduce the results presented here with any microplasma source offering similar characteristics.

2. Sensors

As covered in the introduction, stars tell us not only the story of the universe but also about themselves. More precisely, the light they emit carries information about the substances they contain. Even more precisely, by analyzing the electromagnetic (EM) radiation emitted from a plasma source, the individual species and their concentrations in the plasma can be inferred. The reason for this is, conceptually, straightforward: when an atom or molecule transitions from a higher energy (excited) state to a lower one, the energy difference will, in many cases, be emitted as a photon. As particles can only be excited to certain specific energy states, they are confined to emitting an equally specific set of photons, and while the number of possible transitions may be large, the number of probable ones rarely is. This gives each type of atom and molecule something of a spectroscopic fingerprint, a set of emission lines whose properties identify the particle. With this fingerprint, we can not only identify, but also quantify their presence in plasma far beyond our reach. Amazingly, more or less the same processes that reveal the composition of these massive, far away stars are active in the few cubic millimeters of plasma generated by the SSRR described in the previous section. A notable difference between those stars and the SSRR, however, is that our plasma has an easy to access gas inlet. In theory, then, if we have a gas of unknown composition, we can simply flow it through our plasma and it will emit the spectral fingerprint of its constituents. To turn this into a full-fledged gas analyzer, all we have to do is record and identify the fingerprints. Recording photons, light that is, has been possible for hundreds of years [9] – sorting individual wavelengths and recording their intensity, however, is a bit of a different matter, especially when spatial and power constraints are involved. After all, the miniaturization of the plasma source would be for naught if we were going to strap it into a large array of prisms and lenses. To determine what our options are then, we will have to get into some details of how a spectrometer works.

Most compact optical (visible light) spectrometers are based on two main components: a diffraction grating and a light sensor. The former disperses the wavelengths of the incident light, and the latter records their intensity. The spectral resolution, i.e., the minimum resolvable wavelength separation,

$$\Delta\lambda_{min} = \lambda/\mathfrak{R} \tag{2.1}$$

of a grating at a wavelength λ is determined by its resolving power, in this context

$$\mathfrak{R} = mN \tag{2.2}$$

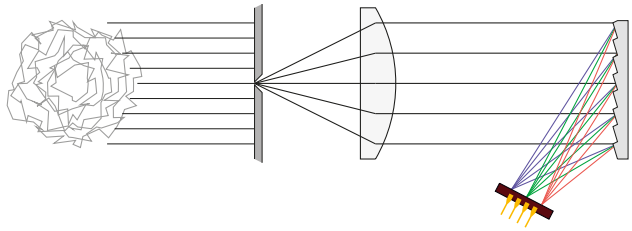

Figure 2.1. Structural overview of a minimal microplasma and spectrometer-based gas analyzer, starting from the left with the plasma emission which passes through a slit, then a collimating lens, hits the diffraction grating, and is recorded by a CCD.

where m is the diffraction order and N the number of illuminated grooves on the grating. In addition to resolution, its descriptive opposite, i.e., the maximum resolvable wavelength separation, is defined by the *free spectral range* and given by

$$\lambda_{fsr} = \frac{\lambda_{min}}{m} \tag{2.3}$$

where λ_{min} is the shortest wavelength in the range. While there are several other properties of a diffraction grating, and the required optical system, that affects the performance of an optical spectrometer, the ones laid out above highlight one key issue; increasing the wavelength range decreases the spectral resolution. Also, as the diffraction order increases, the intensity of the dispersed peaks decreases. Going back to our spectral fingerprints, this means that as the range of recordable fingerprints increases, not only does their sharpness decrease, but the contrast as well. The latter, however, can to a certain degree be addressed by using a more sensitive sensor.

At the time of writing, the most common sensor used in compact optical spectrometers are linear image CCDs, with the main alternative being linear image CMOS sensors[1]. While the latter completely dominates the sensor market for small portable cameras, the properties required for a spectrometer differ significantly from those of, for example, a phone camera. Regardless of what type of sensor is used, the key features of it are its spectral response, full well capacity (FWC), pixel width and pitch, and – as with any sensor – the signal-to-noise ratio (SNR). The spectral response, often described as the sensitivity of the sensor, is in its most basic form simply quantum efficiency (QE), i.e., the ratio of number of signal electrons to incident photons. In a data sheet, however, it is often given in units of A/W (nonlinear conversion from QE) or V/(lx·s) (clamped nonlinear conversion). As the name suggests, this is a wavelength-dependent feature of the sensor, with commercially available back-illuminated CCDs focused on high sensitivity in the visual range reaching above 95% peak QE around its 500 nm center wavelength and about half that at

[1] Indium gallium arsenide (InGaAs) sensors are also available and in general offer faster response times than CCDs. They are, however, currently almost exclusively used in the NIR range.

the edges of the range. While similar peak QE level CMOS sensors have been demonstrated in literature, commercially available ones are still lacking. Similarly, the FWC, i.e., the number of electrons a single pixel in a sensor can hold, of both research and commercial[2] linear image CCDs tend to be significantly higher than corresponding CMOS sensors [10, 11]. It should be noted that in the context of a spectrometer, increased sensitivity, in most instances, requires an increased FWC as saturating individual pixels on a sensor not only causes information loss but also blooming, a process where signal electrons spill into adjacent pixels, inflating the intensity recorded by them. FWC, however, is in general, a simple higher-number-is-better property.

Finally, the pixel width and pitch is a feature that has to be matched with the angular dispersion of the grating, i.e., the angular separation per unit range of wavelength,

$$\mathfrak{D} \equiv \frac{d\theta_m}{d\lambda} = \frac{m}{a\cos\left(\theta_m\right)} \tag{2.4}$$

where a is the center to center distance between two adjacent slits in the grating, and θ_m the angle of diffraction order m. Hence putting further restrictions on the physical design of the system, and requirements on the supporting optics. Ways to circumvent many of these requirements to achieve miniaturized spectrometers is the subject of active research [12, 13], unfortunately, none are yet available for general use.

Knowing then, that when constrained by size and portability requirements there is a trade-off to be made between spectral resolution on the one hand and wavelength range and sensitivity on the other, we are forced to make a choice in how many fingerprints we want to be able to record and at what resolution and contrast. So from now on, we will simply focus on one, meaning we will, instead of trying to determine the species and concentration of all parts of a gas mixture, we will zone in on one of them. To do this, there are two general approaches we could take. We could just select one single emission line (so a single part of a fingerprint), and get a narrow range, high resolution spectrometer centered around that specific wavelength. The process of determining how the intensity of this line relates to the concentration of the species it belongs to would then simply be to record the intensity for a set of varying concentrations. Nice and easy, just like figure 2.2a shows. However, with this approach, it is hard to account for emission line superposition, i.e., where other species has one or more emission lines at wavelengths closer to the selected one than the $\Delta\lambda_{min}$ of the spectrometer, or spectral overlap stemming from line broadening [14]. If we then were to describe the microplasma and spectrometer together as a sensor, this would mean that the specificity (ability to respond to only a single species) of it would not be very good. Low specificity does not imply

[2]In commercial data sheets the FWC, or even the saturation voltage (V_{sat}), is rarely specified. Instead, the dynamic range is given as the ratio between the FWC or V_{sat} and the readout noise.

that it is a bad sensor, only that the range of applications it can be deployed in is limited.

Using a bigger $\Delta\lambda_{min}$ but wider range spectrometer would, of course, increase the number of superpositioned and overlapping lines, but it would also be able to record multiple emission lines, i.e., a larger portion of the spectral fingerprint, of the sought after species. Additionally, it would make it possible to investigate the indirect effects of exciting the gas we are looking for, such as emission lines from species resulting from molecular disassociation (the splitting of molecules, $CO_2 \rightarrow CO + O$ for example) in the plasma. At first glance, with these added wavelengths and thus more information, it might seem intuitive that we should be able find out more about the plasma and its constituents. However, that is not considering the part we swooped by with just a quick reference to figure 2.2a before – the part where we employ a curve fitting method to find a relation between our two measured values. The method we invoked will during execution treat one of the measured values as an independent variable and the other as a dependent one. By convention, the dependent one, the one we want to predict with the function provided by the curve fit, is placed on the vertical axis, so also in the figure. The issue that arises when we start adding more independent variables, in this case wavelengths, is one of *sampling density*. Let's illustrate it with an idealized example of the small $\Delta\lambda_{min}$ approach, but we will express it a bit more formally; We know that the intensity of exactly one wavelength in the plasma emission spectrum relates to the concentration of a species we want to measure. Given that the spectrometer records the intensity at this single wavelength in a [0, 1] range of arbitrary units, AU, and we record 11 equidistant intensities, we have sampled the one dimensional *feature space* – here *wavelength space* – such that no two adjacent measurement points are further away from each other than 10^{-1} AU. When we now employ the curve fitting method, likely a linear least squares one, we provide it with a feature space with a sampling density of 11. Looking at the resulting curve this is likely enough for us to confidently assume that we can later measure an intensity of this wavelength and predict the concentration of our species (with all the caveats listed above, of course).

Before we continue, it might be worth mentioning that this example is a bit contrived, as what we are likely to do is to measure the intensity for 11 equidistant concentrations rather than intensities, but let us assume that we designed the experiment this way.

Now, should we realize that the species we are interested in has another emission line that provides further information about the concentration, we might be tempted to simply divide our still one dimensional *output space* – here *concentration space* – into to 11 equidistant steps and perform new measurements. Looking at it from our curve fitter's perspective, it has then been tasked with fitting a continuous surface to 11 points of semi-unknown distribution, that is shaped like the one outlined in figure 2.2b – a challenge, to say the least. So what we need to do to retain the sampling density, is to measure the

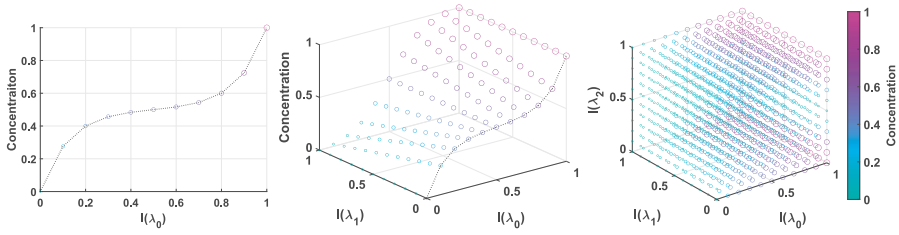

(a) 1D feature space. *(b)* 2D feature space. *(c)* 3D feature space.

Figure 2.2. Exponential increase in samples required to retain sampling density as the number of features increase.

concentrations for 11^2 equidistantly distributed intensity combinations. Even ignoring the complexity of setting up this kind of experiment, we have just significantly increased our required lab time, going from 11 measurements to 121. Well, maybe not significantly, if we can automate the mixing of our gas and use a high frequency CCD, we could record thousands of samples every second. However, this process of adding more wavelengths to a measurement generalizes to the number of samples we need to record being $10^{n \cdot m}$, where n is the absolute value of the exponent of our adjacent sample distance, and m the number of wavelengths per sample.

To concretize this using real-world hardware, we can look at the high speed CCD S15729-01, capable of reading up to 70 000 spectra of 2048 pixels per second. To map the wavelength space for the spectrum it can output at an adjacent sample distance of 10^{-1} AU, we would have to record 10^{2048} spectra (with corresponding concentrations). This is roughly 10^{1960} more samples than there are atoms in the universe, thus posing an issue for storing the data. Furthermore, it would take around 10^{2036} years, which is at least 10^{2020} years longer than the universe is projected to support any form of information processing [15].

This general issue – the exponential increase in samples needed to retain the sampling density of a feature space – is what Bellman called *the curse of dimensionality* [16]. He did, however, also chipperly note that there is no need to feel discouraged by it, as it has been affecting physicists and astronomers for many years. What this means in practice is that the wavelength space we operate in when recording the spectra will be very sparsely sampled. This, in turn, forces us to employ statistical methods to find a reliable approximation of the relationship between a recorded spectrum and the concentration of a sought after species.

2.1 Regression Analysis of Spectral Data

Before getting into the details of any analysis, it is worth spending a little time introducing the nomenclature used here and how it relates to that of the cited work. To do this, we start with the most general description of the regression task at I mentioned earlier, which is to employ a statistical method to approximate a function f such that $\mathbf{Y} = f(\mathbf{X})$, where $\mathbf{Y}$ is an $N \times 1$ matrix where each row, y_i, contains an observation of the dependent variable, and $\mathbf{X}$ an $N \times M$ matrix where each row, x_i, contains the corresponding observation of the independent variables, x_i^j, for $i \in [0, N]$ and $j \in [0, M]$. What differs here from much of the cited work is the superscript index j for independent variables (IVs), as well as using the term IV instead of predictor variable, regressor, explanatory variable, input variable, parameter of $\mathbf{X}$, or any of the numerous other terms found in literature. The former choice was simply to maintain consistency throughout the thesis, such that v_i is always the ith observation of variable v. The latter was chosen partly because of how some of the other terms are used to mean different things in different publications, e.g., predictor in [17] and [18], and partly by personal preference. Additionally, I use the term dependent variable (DV) rather than response variable, regressand, outcome, output variable, or numerical response for the same reasons.

With this clarified, revisiting the leftmost panel in figure 2.2 makes it apparent that for the case of $M = 1$, making a least squares fit of a function to the observations is a distinctly surmountable task. However, even in this case, the issue of finding the correct underlying physical relationship becomes apparent. Any number of functions can have its parameters adjusted such that the sum of squares of the residuals between the function and the 11 values in the figure is adequately small, but finding the one that truly models the relationship between the intensity of the emission line and concentration of the species is a task that requires extensive knowledge about the underlying physics. What is further shown by the figure is that adding more wavelengths will not only cause the feature space to be sparsely sampled, but it makes deducing anything about the underlying physics, using only the least squares method, anything but feasible – hence the popular aphorism *All models are wrong* [19]. Additionally, collinearities, or multicollinearities, among the IVs can often cause severe instabilities when trying to fit a function to observations using the linear least squares method. Collinearity, in the perfect case, is when some IV can be expressed as $x_i^j = \gamma_0 + \gamma_1 x_i^k$ (for multicollinearity, the linear relation is to more than one other variable), where γ_0, γ_1 are constants and $j \neq k$, for all $i \in [0, N]$ and is of course quite uncommon in experimentally obtained data. However, even less than perfect correlation between IVs have a negative effect on fitting, which poses an issue for spectral data where this is known to be the case. Especially affected are molecular emission spectra since most molecules have a large number of allowed energy states, making their emission lines form entire emission bands [20, ch 1.3, 1.4].

At this point, it may be worth connecting the generic expressions above more closely to the application introduced in the previous section. Given that we seek to approximate a function that predicts the concentration of some species in our plasma given its emission spectrum, y_i will be a measured (observed) concentration of that species. The corresponding observation x_i will thus be the spectrum emitted from the plasma at that concentration, and followingly x_i^j the intensity of jth wavelength in that spectrum. This, in turn, means that N would be the number of spectra and corresponding concentrations recorded in the experiment, and M the number of wavelengths in each spectrum – i.e., pixels in the CCD of the spectrometer.

The by now high dimensional curve-fitting is, for us, further complicated by the fact that it is known that not all intensities correlate with the concentration of the sought after species. This could be handled by adding weights to the curve fit, making parts of the spectra known to not contain primary emission lines less influential in the fit, or even completely removing them. This would, however, negate most of the reasons for opting to use a wider range spectrometer in the first place. A better way would thus be to analyze which parts of the spectra vary with the concentration.

> To avoid simply switching between terms here, it is worth noting that, to the best of my knowledge, there is no clearly defined difference between curve-fitting and regression. As a personal preference, however, I tend to use the expression *fitting a function* to a set of observations when the independent and dependent variables look, but are not known, to be correlated, and *regression analysis* when they are. As we know that the emission spectrum from the plasma is correlated to its composition, I will now switch to using the term regression.

In an effort to address both sparsely sampled feature spaces and collinearities, and with the assumption that processes that generate recordable data are in general driven by a small number of hard to measure variables [21], Wold et al. developed partial least squares, a.k.a. projection to latent structures, (PLS) regression in the early 1970s [22]. Originally intended for the social sciences, it has since become widely used in several fields, not least chemometrics. PLS works by generating a set of uncorrelated linear combinations of the IVs, the so-called latent variables (or score vectors), that are then used to perform a least squares regression. This projection of the observed data to a latent space can, to a certain extent, be controlled by limiting the number of variables the method should generate. The, arguably, most important aspect of the process for the spectral application discussed here, is that it leads to a biased but lower variance estimate of the regression coefficients by, as a virtue of the algorithm rather than manually, assigning larger weights to IVs with high variance when creating the latent variables. Thus, it makes it possible to design experiments

to, theoretically, increase the chance of the method to model the physical relation between the spectra and the concentration. However, as is shown in **Paper V**, the limitation of restricting the dependent variables to a linear combination, even of latent variables, can adversely affect the predictive performance of its models – clearly so when the true relation between the independent and dependent variables is, in fact, nonlinear. There have been multiple nonlinear extensions to PLS [23] developed since its inception. Most of them can be categorized by when the nonlinearity is introduced: after the latent variables have been created [24], during the calculations of them [25], or by a nonlinear transformation applied directly on the independent variables [26]. While all three categories are able to improve regression on select data sets, it is hard to interpret the transformation in the first two from a physical point of view when dealing with emission spectra. For the last, the transformation $\Phi\left(x^j\right)$ is essentially an idealized version of one or more optical components. In slightly more formal terms, Φ nonlinearly maps the original IVs to a feature space where a linear PLS model is created. While the details of this method lie outside of the scope of this thesis, this structural overview will hopefully suffice as a basis for comparing the models of these methods, i.e. their approximations of the function f mentioned in the beginning of this section.

Another family of regression analysis methods that, to quote the book The Elements of Statistical Learning [27, ch 10.3], "*there has been a great deal of hype surrounding [...], making them seem magical and mysterious*" are neural networks (NN). Structurally, the basic version of a neural network is quite similar to PLS – a set of intermediate features are derived from the IVs that are then used to model the DVs through linear combination. Despite this similarity, the underlying assumptions of the methods differ in a substantial way. Where PLS tries to find the hidden driving features of the data generating process, NNs build on the idea that a sufficiently advanced network of hidden features, misleadingly named neurons, is able to approximate complex relations between independent and dependent variables. For a more detailed comparison of how the latent variables of PLS and the neurons of the NN used in **Paper V** are iteratively calculated, see reference [28] and [29], respectively. There are at least two things to note about this comparison. Firstly, the PLS reference provides the full details on how to go from having a matrix of independent variables, **X**, and a dependent one, **Y**, to making predictions on new observations – the NN one only describes the algorithm used for the optimization of an objective function. For our application, the objective function, $f(\theta) = N^{-1}\sum_i^N (p_i(\theta) - c_i)^2$, is simply the mean square error (MSE) between the predictions of the NN model, p_i, and measured concentrations, c_i, and the parameters (which are in the same paper also called weights), θ_i, the coefficients of the linear combinations of IVs that make up the intermediate features. Secondly, PLS is an end-to-end defined regression method, while neural networks, even when only considering regression versions of them, are more of a type of architecture of methods where it is possible to select and

replace individual parts. So essentially, this comparison is the same as comparing a classic novel, written by a great author, with what I came up with in a *pick your own adventure* book. It does, however, highlight some of the clear structural differences between the methods. Because while it is technically possible to select the nonlinear transformation, Φ, in the kernel-based PLS method, neural networks make the selection a core part of employing the method, and the literal multilayered approach of NNs creates an additional nonlinear transformation that is learned from the input data, rather than selected. The modular nature and numerous parameters (or hyperparameters as they are regularly called) of NNs have some distinct downsides as well, one being the barrier of entry they create. Another is the almost complete lack of interpretability of any intermediate representation of the input data. All of this, together with the tuning of parameter values that is often required, makes it hard to compare the predictive performance of models stemming from the different methods – for one thing, how much tuning of a model is *fair*? at what point in the tuning should the method simply be considered a bad fit for the application? Nonetheless, it is very much possible to make a minimum viable version of a neural network, one that only has a small number of parameters to tune, all of which can be safely left with some sensible default values. With a small number of neurons, it would even be fast to train. Having few neurons, however, will cause the performance of such a model to depend heavily on the training data provided, an artificial shortcoming not present to the same extent in PLS-based methods. To work around this, and thus try to compare the *approach* of PLS with that of neural networks, it is possible to use an ensemble [18] of small NNs, and in that way remove the aforementioned barrier, on our regression task.

2.1.1 An experimental design for method comparison

In addition to the considerations concluding the previous section, an aspect of primarily the nonlinear methods that needs to be taken into account in a comparison is the computational resources required. While a method, tuned or not, might be able to model complex physical relationships, its usefulness still decreases rapidly as computational time and resources increase. With all of this in mind, the approach taken in **Paper V**, where the three methods discussed above were compared and evaluated, was to compare them from what could be described as an experimentalist's perspective. That is, the experiments to collect spectra and CO_2 concentrations were the ones tailored to the specific regression task, rather than the parameters of the methods. The evaluation then sought to determine the methods' dependence on preprocessing of the spectra, feature (i.e., wavelength) selection, and training set size (N). While preprocessing, in general, can encompass quite extensive analysis on its own [30], it was limited to two basic noise reduction methods, standard normal variate

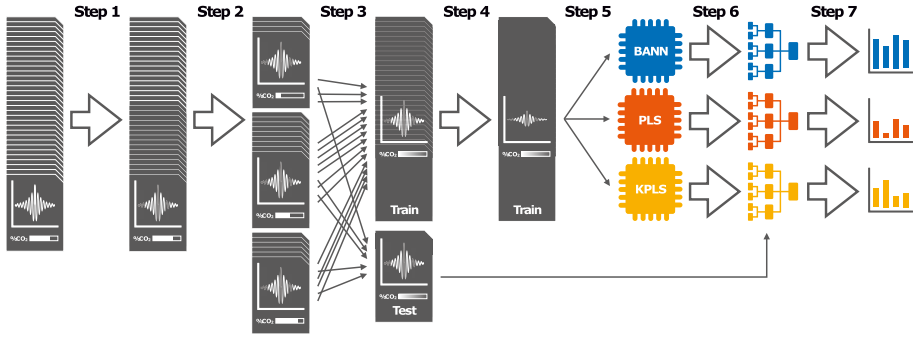

Figure 2.3. Structural steps of training and testing models in **Paper V**. The leftmost stack represents all of the acquired spectra together with their metadata, and the following steps are (1) feature (wavelength) selection, (2) concentration based binning, (3) randomized bin- and acquisition group based train-test split, (4) preprocessing, (5) training, (6) testing, and (7) generating evaluation metrics. Each model was generated with this pipeline 4 times.

(SNV) correction and sample averaging. This was intended to investigate the sensitivity to IV noise of the produced models. In a similar vein, the feature selection was used to evaluate the methods' ability to model latent spectral information outside of the primary emission lines, as well as to discard sections of the spectra that carried no such information. This was differentiated from the preprocessing as it had a direct effect on the SNV correction and because the subsets could be reproduced by simply using a spectrometer with a narrower spectral range.

I consider the methods' dependence on these three aspects generic enough to provide a strong indication of how they would perform on the same regression task for a different species with similar relative emission line strength. A caveat to this is the most prominent application-specific concession made in the study, which was the concentration range, 0.1% to 4%, meaning that the conclusions drawn are limited to a relatively weak signal. This limitation did, however, not affect other parts of the experiments. The train-test-evaluate pipeline shown in fig. 2.3, does contain a non-generic design choice as well though. In step (2), where the observations are grouped into 5 concentration bins (the three bins in the figure are just for visualization purposes), from which the random train-test splits were drawn meant that a model's test set could contain spectra that required it to extrapolate from its training data. This could, of course, have been circumvented by always placing observations of the lowest and highest concentrations in the training set. In the study, however, a model's ability to extrapolate up to 20% outside of its training range was considered of interest. Furthermore, the train-test split in step (3) was, in addition to concentration, based on the so-called acquisition groups. These groups corresponded to a constant CO_2 concentration and spectra recorded under as close to constant ambient conditions as the setup offered. To avoid a situation where a model

would essentially be tested on spectra that were also present in its training set, all spectra within a group were ensured to only be placed in either a train or test set. While this could be considered an experiment-specific consideration, I am hard pressed to imagine an experimental design for a similar comparison that would not contain an analogous step.

Besides the aforementioned two steps, the pipeline is completely data and regression method agnostic. The three chip-like symbols in the figure represent the methods evaluated in the paper, BANN for the neural network ensemble, PLS for the method with the same name, and KPLS for the nonlinear, kernel-based version of PLS mentioned in the previous section. The following horizontal network symbols represents the models that the methods produced. The subsequent evaluation step, while data and method agnostic, evaluated the models' predictions as if they were the output of a sensor.

2.1.2 Evaluating regression models as sensors

When evaluating the *goodness of fit* of a regression model, one of the most commonly used statistics is the coefficient of determination, R^2. While there are several definitions of it [31], the one employed in **Paper V** was

$$R^2 = \max\left(1 - \frac{\sum_i^N (\hat{p}_i - c_i)^2}{\sum_i^N (c_i - \bar{c})^2}, 0\right) \tag{2.5}$$

where $\hat{p}_i$ is the ith prediction given by a linear regression of all the predictions, p_i, by the model, c_i the ith concentration[3], and $\bar{c}$ the mean concentration of the N observations in the test set, i.e., the number of observations selected to evaluate the model on. Expressed in general terms, this is a measure of how well the predictions correlate with the corresponding concentrations. The reason for clamping the value at 0 rather than letting a higher prediction MSE or lower concentrations variance give a poorly predicting model a negative value is that, when interpreting the predictions as the output of a sensor, there is little meaning in a value less than 0. A sensor that outputs a constant signal is neither worse nor better than one that outputs noise.

A consideration that is required when using R^2 in general is that it is based on the assumption that the variance of the target values, for us that would be the concentration, is known. When the values are actually measured or approximated, as in **Paper V**, this is not fully the case. An alternate approach to

[3]In a general setting $\hat{p}_i$ is often also called modeled, fitted, or calculated value, and c_i the true, target, measured, or observed value. To make things more fun they are also often denoted with $\hat{y}$ and y, but sometimes f and y, and other times, other things. My notation might look funny and this is by no means an authoritative text on statistics, but with regards to nomenclature, there clearly does not exist such a thing.

evaluate our models' predictions is to treat the measured and predicted values as two separate datasets and measure the correlation between them. The measure used for this in the paper is Pearson's correlation coefficient (PCC) which is given by

$$\text{PCC} = \frac{\text{cov}\,(p, c)}{\sigma_p \sigma_c} = \frac{1}{N-1} \sum_{i}^{N} \left(\frac{p_i - \bar{p}}{\sigma_p} \right) \left(\frac{c_i - \bar{c}}{\sigma_c} \right) \tag{2.6}$$

where $\text{cov}(p, c)$ is the covariance of p and c, σ_p and σ_c the standard deviation of the predictions and concentration, respectively. With this approach, a negative value does make sense; we have one sensor that outputs a model's predictions, and we have another that we measured the concentration with beforehand. With the PCC, we then explicitly handle them both as sensor output, rather than treating the latter as a ground truth.

As both R^2 and PCC are only measures of the correlation between a model's predictions and the measured concentrations, if we are interested in the trueness – which is what the International Organization for Standardization (ISO) calls what is more commonly referred to as accuracy [32] – of them, we need an additional measure. The most straight-forward measure of this is of course the (root) mean square relative error, the relative part then takes care of comparisons between top- and bottom heavy test sets. This is, however, where the concentration range and measurement method used in the study imposes some extra requirements on the evaluation. At the lower end of the former, there will be CO_2 emission lines that are simply swallowed by the broadening of adjacent lines – thus making predictions in this lower concentration end harder than just predicting at a lower SNR. With regards to the latter, the gas concentration was measured by dilution of a standard. Therefore, lower concentration samples that had been diluted more times had a greater concentration uncertainty and could thus introduce artificial errors in the predictions. To account for the above, we added relative concentration-based weights to the RMSRE, arriving at a prediction error term defined as

$$\text{wRMSRE} = \sqrt{\sum_{i} w_i \left(x_i - y_i \right)^2} \tag{2.7a}$$

$$w_i = \frac{1}{N_t} \frac{y_i}{y_{max}} \tag{2.7b}$$

where w_i is the ith weight, N_t is the number of values in the training set, and y_{max} the maximum concentration in it.

When employing these three measures as a compound score, $\frac{1}{3}\left(R^2 + \text{PCC} + 1 - \text{wRMSRE}\right)$, we found that it was dominated by the third term, and biased towards models that would perform well on low concentrations but not provide anything useful at higher ones. To rectify this, we introduced a scaling term, in the paper dubbed the *positive trueness parameter*.

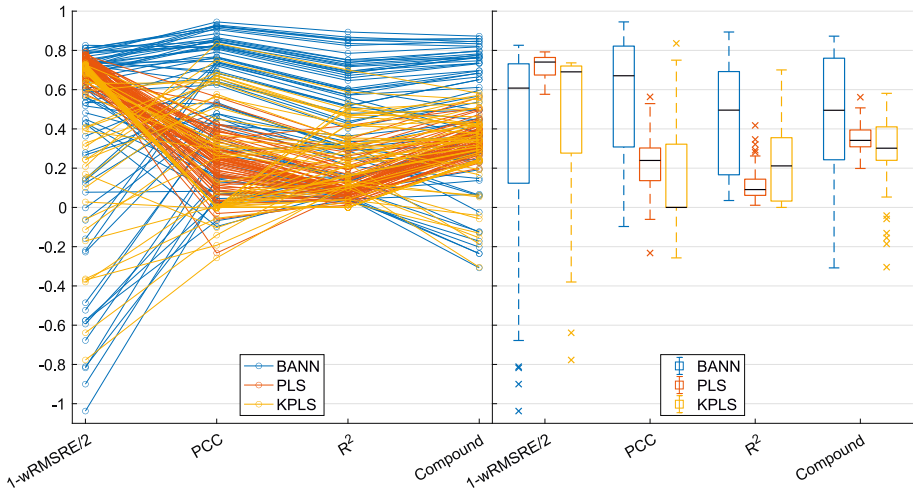

Figure 2.4. All values of all measures used to evaluate the models in **Paper V**. In the boxplot to the right, the black lines indicate median values.

As it only scaled the wRMSRE value, it had an intuitive interpretation as the inverse of the largest relative error that would positively contribute to the compound score – i.e., it functioned as a numerical threshold for what was *good enough*. With this, the final compound score was defined by as $\frac{1}{3}\left(R^2 + \text{PCC} + 1 - p_{\text{pt}} \cdot \text{wRMSRE}\right) \in (-\infty, 1]$ and the different models could be compared.

As shown in figure 2.4, the value of p_{pt} was set to 1/2 – meaning that an average relative error of less than 2 gave a positive contribution to a model's score. Additionally, the figure highlights how the measures complement each other. The left pane, in particular, shows that while a low R^2 value may be sufficient to discard a model, it is decidedly insufficient to compare multiple ones.

Finally, in figure 2.5, the mean compound score of each individual model is color- and size coded with the training set size on the horizontal axis. This is what I believe to be the most interesting result of the study, as it provides a clear view of which configurations of the regression methods that were able to benefit from an increasing number of training samples – a strong indication that the method is approximating the underlying physical model. While the BANN models consistently performed significantly better than the other two methods, as long as SNV corrections where not in the pipeline, the trend of prediction performance scaling with training set size can also be seen with some KPLS configurations.

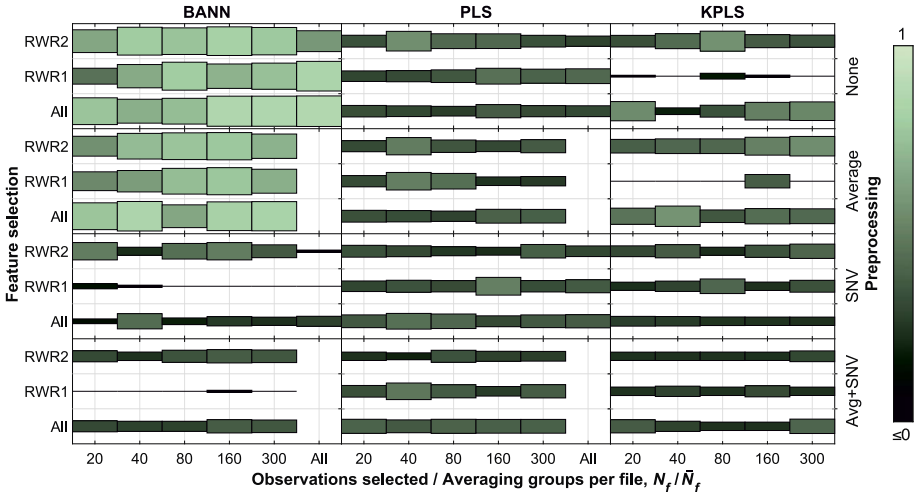

Figure 2.5. Mean compound score for each model represented by the color and height of its box. Higher and brighter boxes indicate a score closer to 1, a single pixel line a score $\leqslant 0$, and an empty slot means no model was trained for the combination parameter values.

2.1.3 Out of domain predictions

In an additional study to **Paper V** that was not included in the final publication, the best performing model of each regression method, as measured by the compound score, was put to task on what is usually referred to as *out of domain* data. This was simply spectra recorded using a setup that is covered in the next chapter. For the purpose of evaluating the regression methods as part of a sensor, the vertical lines in figure 2.6 indicate when the gas flowing to the plasma was switched between a higher concentration source (on) and a lower one (off). The difference, compared to the previous experiments, was that the composition of the gas was not controlled – it was the ambient air in the lab – only the timing of the changes in CO_2 concentration was known. From this, we are still able to discern several interesting properties of the regression models; The BANN model seems to indeed approximate the relationship between the plasma emission spectra and its CO_2 content. The change in baseline between the two repetitions was to be expected, and thus reinforces the conclusion. The PLS model on the other hand, did provide low variance predictions but did not approximate the CO_2 concentration. It *may* have modelled something related to it, but even that, it did inconsistently (see day 2, prior to the first off-line). The KPLS model suffered the same inconsistency as its PLS cousin, though otherwise getting the relative changes correct. But comparing the two repetitions shows that it was much too sensitive to the overall gas composition to offer any value as part of a gas sensor.

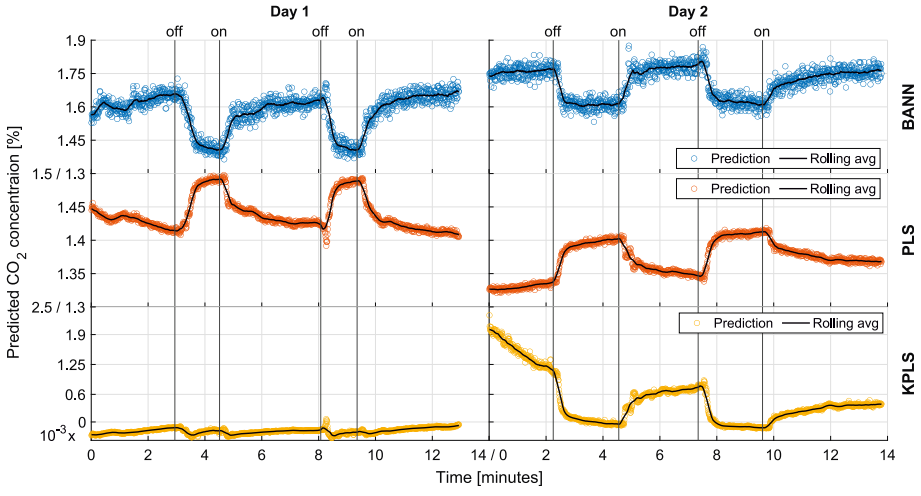

Figure 2.6. CO_2 concentration predictions of the best performing regression models on transcutaneous blood gases (see chapter 3). The rolling average has a centered window of 20 seconds and the vertical lines indicate when the plasma inlet was connected to a gas collector placed on the skin of one of the authors (on), and when it was removed from it (off).

2.2 Single peak differential gas sensor

As made clear above, microplasma emission spectroscopy can be used to detect minute relative changes in the composition of an analyte. This makes the technique a perfect candidate for differential gas sensing. Such a sensor, as the name implies, is one that measures the difference in concentration of the same species between two analytes. Differential sensors in general are somewhat common, a natural example of it is the pressure gauge you use when inflating the tires on your car or bicycle. When it is showing zero it does not indicate that there is a perfect vacuum in your tire, but that the difference in pressure between the ambient that inside the tire is zero.

A spectroscopy-based differential gas sensor, then, is one that inherently only needs to analyze the emission line(s) of a single species. This implies that the analysis could look more like the less involved one in the leftmost pane in figure 2.2. However, fully isolating a single emission line, as discussed in section 2, simply moves parts of the complexity of the system to the hardware side of things. To avoid this, the differential gas sensor presented in **Paper VII** completely forgoes the spectrometer, and thus the grating. The setup, seen in figure 2.7, replaces the spectrometer with an optical filter (green rectangle in the figure) and a photodetector. The operating principle of the sensor was to turn the two plasma sources on and off perfectly out of sync, such that the photodetector would only be illuminated by one of them at a time. Thus making the signal from it take the shape of a square wave, the amplitude of which corresponding to the difference in concentration between the samples in the

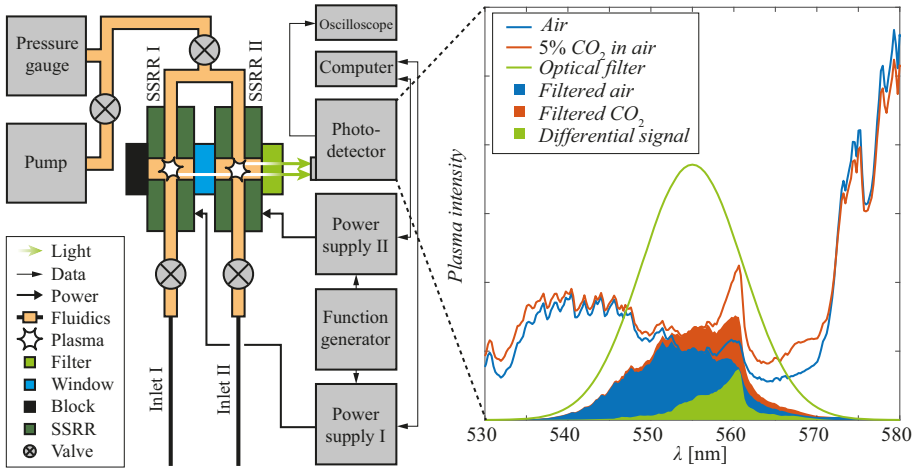

Figure 2.7. Differential gas sensor setup from **Paper VII**. The left panel shows the two microplasma sources, with individual gas inlets and a shared outlet. On the right is an overview of the transmitted light recorded, and in essence summed up, by the photodetector.

plasmas. As seen in the right part of figure 2.7, the optical filter chosen for the study had its central wavelength close to one of the most prominent CO emission bands in the optical spectrum, indicating the focus on CO_2 measurements in this study as well.

Given its prominent use cases, such as calibration and diffusion measurements, two of the most important properties – aside from accuracy – of differential gas sensors are stability and response time. While the latter is an unambiguous measure, the former is often described as the absence of drift. To quantify this, the bottom half of figure 2.8b shows the Allen deviation, σ_A^2 over time. The basic interpretation of it is that as long as σ_A^2 is decreasing, averaging samples will improve SNR. This, in turn, means that at the point where the slope of the curve changes sign, the drift of the sensor overtakes the noise. The time it takes to reach this point is known as the *maximum averaging time* of a sensor and is used to denote its stability. As seen in the figure, the sensor presented in the paper has an averaging time of about 620 seconds, which, compared to other types of sensors places it in sparsely populated middle ground. It is lower than the (up to) 1000 s offered by high end, 10 000+ € systems, but significantly better than the sub-100 € sensors that tend to drift off around the 3 minute mark. With an expected bill of materials cost below 500 € for a final sensor, which will have explored the ample room for optimizations of the current preliminary design, and similar improvements over the cheaper options in response time and accuracy, see figure 2.8a, the sensor presented in the paper is likely to provide medium range option where there was previously none.

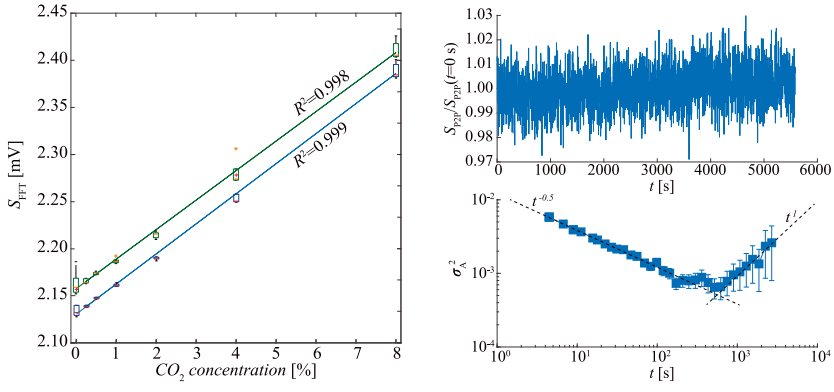

Figure 2.8. The left panel shows the correlation between the two modes of peak intensity analysis and CO_2 concentration. The right one the stability of the system as expressed by the Allan deviation.

3. Systems

It is often said that a good system is more than the sum of its parts – a corollary to this would be that designing a good system is harder than simply putting good parts together. So while the sensors described in the previous chapter are able to detect and compare minute gas concentrations, that is a far cry from a complete system for residual gas analysis. The design of such a system is, of course, entirely application dependent. Therefore, in the following chapter, I will focus on a system intended for a very particular application, namely blood gas monitoring on premature neonates.

Blood gas monitoring is the process of measuring the amount of CO_2 and O_2 in the blood of a patient, and provides vital information about the respiratory and circulatory functions. This is particularly important in the neonatal care of prematurely born infants, as their hearts and lungs are not ready to support them outside of the womb. However, far from all neonates that needs this care gets it. The World Health Organization (WHO) reports that an estimated 15 million babies are born preterm [33] , defined as less than 37 completed weeks of gestation, which is more than 1 in 10. The complications that follow are so severe that globally, prematurity is the leading cause of death among children under the age of 5 years [34]. As with most health care-related issues, the vast economic inequalities around the world play a dominant role in deciding which prematurely born children get to live and which will die. In the affluent part of the world, the death rate of extremely preterm babies (less than 28 weeks of gestation) lies around 10%. The corresponding number in countries still suffering the economic and social consequences of colonialism, enslavement, and wars driven by the aforementioned affluent ones, is 90%.

One of the many reasons for this acute disparity is the lack of available, affordable, and portable medical equipment. This, in turn, is one of the primary reasons why the research described below has been performed using, to a large extent, off-the-shelf components and focuses on fabrication methods that do not require access to cleanroom facilities.

3.1 Transcutaneous Blood Gas Monitoring

Pulmonary complications (issues with the lungs) are one of the most common issues for premature neonates. The acute risks of hypoxemia (low blood oxygenation) and hypercapnia (high CO_2 concentration in the blood) that is associated with these complications are in adult patients monitored by their general

condition and clinical signs such as flushed skin, rapid breathing, and involuntary muscle contractions. Diagnosing the conditions is done by simple blood sampling. For premature neonates, almost none of this is possible; drawing blood is associated with a large number of risks [35], and the possibility to do so at all is limited by their small blood volume.

The primary alternative to blood sampling for blood gas monitoring is a technique called transcutaneous (through skin) blood gas monitoring (TBM). As the name suggests, it measures the concentration of CO_2 and O_2 that permeates the skin, with many of the commercially available solutions marketing themselves as *trending tools*, i.e., measuring relative changes in the concentration rather than absolute values. The sensors used by these systems were developed in the 1960s [36], with first clinical systems taking another two decades to be developed [37]. The TBM systems in use today have been optimized but still rely on skin-mounted sensors that will filter out the gas species of interest using a thin membrane, after which the equilibration of the partial pressure of the remaining gas and an analyte enclosed in the sensor changes the latter's pH which, in turn, is registered by an electrode [38]. This rather complex working principle makes the devices costly, creates a need for frequent calibrations of the sensor using standard gases, and, combined with the slow diffusion rate of both CO_2 and O_2, makes the initial response time of the system, i.e., the time from sensor mounting until a stable signal is acquired, be measured in tens of minutes. To increase diffusion, most sensors incorporate a heating element. The downside of continuous skin heating is that the exceptionally sensitive skin of premature neonates is significantly more susceptible to burns compared to that of adults, which has led the WHO to recommend frequent sensor relocation [39]. This, in turn, poses a significant risk of skin damage as the sensors are generally held in place with adhesive pads, which can easily cause skin tearing when removed. This type of damage has been reported to cause lesions and skin necrosis in babies [40]. Finally, the size of the sensor, the most common type being somewhat cylindrical in shape with a diameter in excess of 20 mm and height of 10 mm, makes it, at the very least, impractical to place anywhere but on the torso of a preterm neonate. This is an area where it will invariably compete for space with other medical devices, some of which with better claims to the surface, such as ECG electrodes.
Combined, these issues make truly continuous TBM on preterm neonates unfeasible and have even called into question the very use of the technique in NICUs [41]. However, the lack of viable alternatives for the vital information they provide has left them in place in the vast majority of modern neonate care facilities of sufficient financial means.

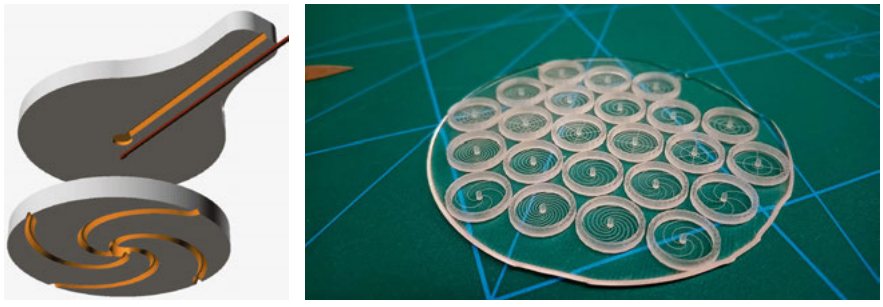

(a) Patch CAD. *(b)* Set of patch molds.

Figure 3.1. 3D model of a patch design and one of many mold sets for the skin-facing part of the patch created to evaluate different designs.

3.2 Micropatterning PDMS

The primary pain points that an alternative approach to TBM would need to address are thus the mounting, size, and stiffness of the sensor. The approach to this taken in **Paper III** was to move the sensor off the patient and replace it with a soft, gas-collecting patch connected to a fused silica capillary that transports the gas to the sensor. It collected the transcutaneous gas through a series of microchannels on the skin-facing side of the patch that convened at a cavity leading up to the capillary, see figure 3.1a.

Developing devices for medical applications comes with a host of well-founded restrictions with regard to the types of materials that can be used, particularly for those intended for prolonged skin contact. Luckily, polydimethylsiloxane (PDMS) is a biocompatible, soft, silicone material that has seen an almost 10-fold increase in its use in medical research over the last two decades[1] – including applications with prolonged skin contact [42]. It additionally accommodated the goal of avoiding high cost/complexity fabrication processes by consistently, and without the need for specialized equipment, being able to replicate extremely fine features [43]. Therefore we could make the patches by first milling out a long-term reusable positive master mold, i.e., a mold shaped like the final patch, using a regular CNC router intended for PCBs, and then double cast the PDMS in it. While this is clearly not a method suited for large-scale fabrication, double casting PDMS and bonding the pieces together requires little more than a steady hand and some patience.

With a clear path for patch fabrication laid out, the next consideration was the system's target patient group. All babies, premature or not, are notoriously non-compliant with instructions on how to move and not, and with the signal of the sensor relying on a steady flow rate of gas, the malleability of the patch could pose a problem. The primary focus of the study was thus on the flow resistance in the microchannels during deformation. In other words, how

[1] Measured by the number of published papers on PubMed on the subject.

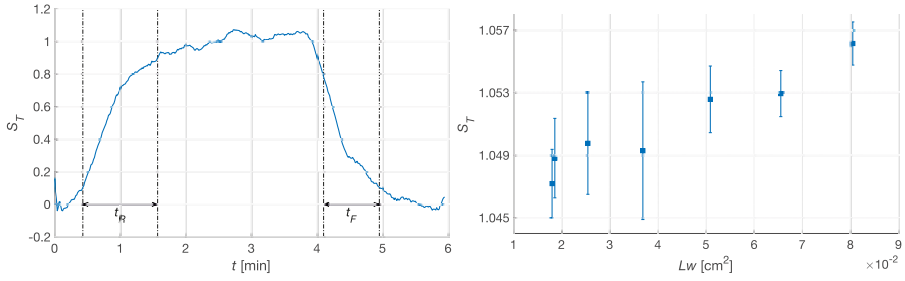

(a) Rise and fall times of the TBM signal. *(b)* Signal strength vs exposed skin surface.

Figure 3.2. Primary results of **Paper III**, showing a significantly shorter signal rise, t_R, and fall time, t_F, compared to state of the art systems and how the signal strength, S_T, increased with exposed skin surface, i.e., the product of the length, L, and width, w, of the microchannels.

to design a patch that ensured that the TBM signal was unaffected by a rambunctious baby lying, chewing, and/or punching on it. To figure this out, we designed a series of different patches of varying channel widths and configurations, a subset of which can be seen in figure 3.1b. We then subjected them to a series of experiments where we put them under uniform and point forces, both from the top and at different angles. The results, as seen in figure 3.2, showed that wider, deeper channels were able to provide a more stable signal as well as sustain bigger loads. Additionally, the proof of concept system reduced the response time to about a tenth of the commercially available system it was compared with.

The wider channels also reduced the concerns about other blockages that may occur. Because while preterm infants, in particular, do not have fully functional eccrine glands (the odorless sweat glands covering most of the human body), and are thus not able to sweat, the glands' postnatal development time on select areas of the body is reported to not be longer than two weeks [44]. So while the 400 µm wide channels in the patch shown in figure 3.3 are unlikely to be immediately blocked by baby sweat, follow-up studies are needed to investigate the risk of it further.

3.3 Electrical Interfaces & Blood Gas Concentration

For all the issues the gas collecting patch solved, its lack of an electrical interface meant that the heating elements and extra sensors incorporated in most conventional TBM sensors were lost. With the limited amount of usable skin surface available on small patients some commercial TBM system vendors have, rather than further miniaturizing their sensors put focus on incorporating other ones, primarily pulse oximetry sensors and thermometers, and with that rebranded their systems as transcutaneous monitoring (TCM) devices. It

Figure 3.3. A fully assembled prototype of the PDMS gas collector patch over a lawn with dandelions.

is worth noting that while these sensors collect important information, they are rarely of the kind that has previously competed for space on baby's torso.

So, with the risk of skin tears removed following the design of the patch, and studies showing that the sustained vasodilation (widening of the bloodvessels) can be achieved by pulsed rather continuous heating [45], **Paper IV** focuses on developing a simple and scalable fabrication technique for a resistive heater that could be integrated into the patches. Since polyimide (the carrier material chose for the heaters), PDMS, and air are all considered thermal insulators, i.e., have thermal conductivity of less than 0.3 W/mK, the heaters needed to be highly efficient to be able to deliver short pulses of heat rather than a slow warm-up. Thus, their design called for the heating elements to be folded into the bulk of the PDMS, reducing the skin-to-heater distance. A popular way of folding Polyimide-Copper laminates, or flexible PCBs or flex as it is most commonly known, into 3D microstructures is laser heating. *Laser origami* [46] as it is called, or *kirigami* [47] when the laser is also used to ablate it, has steadily gained steam over the last decade. While useful when creating proof-of-concept designs, the sequential nature of the technique makes it a poor fit for the heaters, as the patches have to be produced inexpensively in large batches (>10 000 per day) and each patch would have a large number of individually folded elements, see figure 3.4a. Additionally, using a 12 µm Cu-layer flex, the mechanical rigidity of the folds is unlikely to have withheld being cast into PDMS. Instead we devised a novel folding technique based entirely on the surface and viscous forces at play as the PDMS was dispensed over the cut out heating elements, the working principle of it is shown in figure 3.4b.

With the heating elements folded into the bulk of the PDMS, the initial thermal response at the skin surface of a patch was increased by more than a factor of 10 compared to a flat heater. In figure 3.5b, we see the raw thermal data from the comparison at different power levels, which clearly highlights the benefit of the folded design for pulsed heating.

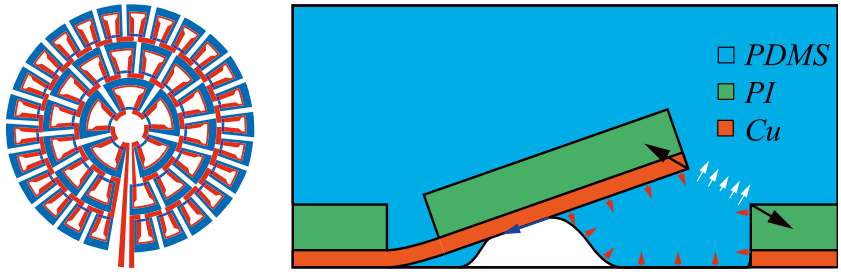

(a) Patch heater design. *(b)* Folding principle.

Figure 3.4. In the patch heater design in *(a)* the copper traces are marked in red and laser cutting outlines in blue. In *(b)* the arrows show the net forces experienced by the individual heating elements during folding.

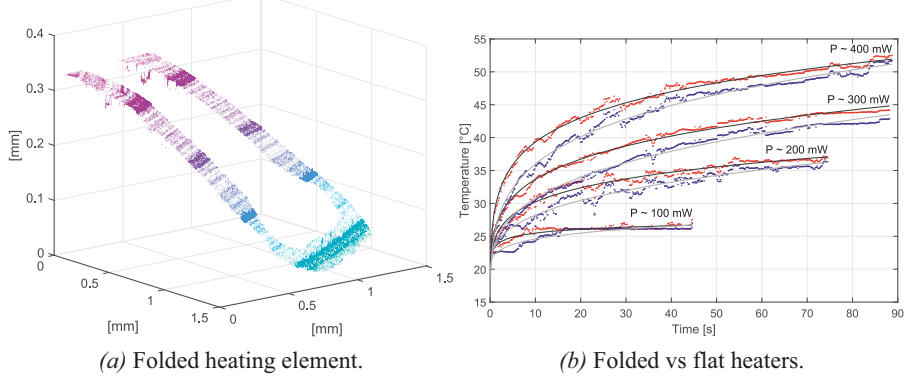

(a) Folded heating element. *(b)* Folded vs flat heaters.

Figure 3.5. Heating element, *(a)*, folded as described by figure 3.4b and measured using an optical surface profiler. In *(b)* the raw temperature data from a heater with its elements folded into the bulk of the PDMS of a patch (red) is compared with that of a flat one (blue) at different power levels.

The heaters have yet to be incorporated into the complete TBM system as there are additional considerations needed with regards to the electrical interface and its integration into the system. Instead, in **Paper VI**, we describe the full TBM system using the passive patch from **Paper III** and a basic spectroscopic sensor together with a theoretical model that relates the measured CO_2 concentration in the transcutaneous gas with that in the blood. The model is based on gas diffusion simulations of the skin and provides an extensive overview of how the different physiological processes in the subcutaneous tissue and blood vessels affect the CO_2 concentration in the diffused gas. In the experiments conducted in the study the measured CO_2 concentration, when based solely on the transfer function derived in the paper, were within 30% of those measured with a commercial device included for reference. When empirical data was used to calibrate the system, the results were within 0.5% of the reference. Although the proposed system showed slightly lower accuracy than the commercial device, it achieved its results without heating the skin, while the reference required an skin temperature of 42 °C. Hence it showed great promise as first step toward a new generation of both simpler and safer TBM for neonates.

4. Actuators

Having explored the implementation and integration of the microplasma as a sensor in a useful system, it is time to look back at the stars where we began. Maybe not all the way out to the stars, but at least some 80 km above sea level. Objects orbiting the Earth at this altitude and up to 2000 km are referred to as being in low earth orbit (LEO), a term that can be confusing given that the *Kármán line*, commonly known as the boundary to outer space, is at 100 km. As seen in figure 4.1 this is the range where a large portion of the currently operational satellites orbit[1].

The three major budget posts of a space mission, e.g. launching satellites into orbit, are generally *(i)* research and development, *(ii)* launch, and *(iii)* mission maintenance including communication with the spacecraft. Neither the first nor last depend much on the the size of the spacecraft, but rather on the specifics of the mission. However, when it comes to the launch, the exponential relation between the spacecraft's mass and required amount of fuel – and thus cost – makes miniaturization an important part of all missions.

By the time they are funded and have made it into LEO, the types of challenges facing satellites vary depending on altitude, but they all have to withstand temperature variations in excess of 100 K and constant particle- and EM radiation. This environment puts harsh requirements on the embedded electronics and even harsher on components on the surface of a spacecraft. Shielding and redundancy are therefore key to ensuring a long lifespan of a satellite,

[1]Data provided by The UCS Satellite Database, v.5-1-2022, `http://www.ucsusa.org/satellite_database`

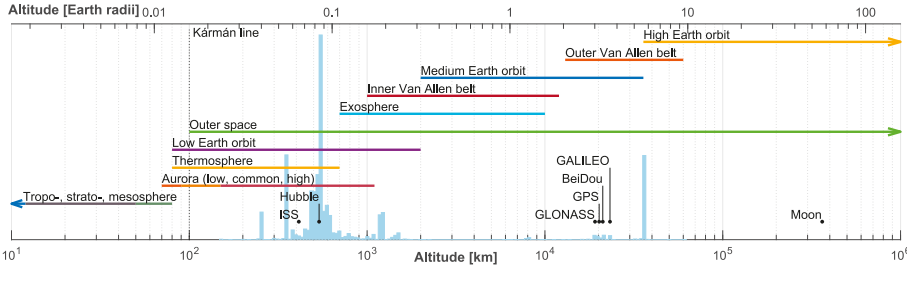

Figure 4.1. Ranges of interest (horizontal lines), notable objects (black dots), and the distribution of the perigee (lowest) altitude of 5467 active satellites currently orbiting earth (bargraph). Note that in an effort to avoid collaboration at all costs, the USA, China, Russia, and the EU have all designed and deployed independent global navigation satellite systems called GPS, BeiDou, GLONASS, and Galileo, respectively.

but even if the unforgiving environment of space can be effectively fended off, there is an unavoidable expiration date – the day they run out of fuel. While losing its attitude control (angular rotation to maintain and adjust orientation) and orbit maintenance ability is not an instantaneous failure mode for all satellites it is, in space, an irreversible state of failing. This is one of the major hurdles limiting mission complexity for miniaturized satellites as the demands on their thrusters are not only ones of extreme efficiency to handle the minimal dry mass, < 1 kg for the nano satellite class – but also to be able to produce low thrust, ~1 mN, at high precision. Several different approaches to accommodate these requirements have been explored [48], including pyrotechnic actuators [49, 50], vaporizing liquid microthrusters [51, 52], and field emission electrical propulsion [53]. Additionally, at ÅSTC, cold gas microthrusters have been investigated and developed over the last quarter of a century [54, 55, 56]. While able to deliver extremely precise, sub-mN thrust, cold gas thrusters – which in its most basic form simply operate by expelling gas to produce thrust – are comparatively inefficient [57]. It should be noted here that comparing the efficiency of microthrusters is a less straight forward process than their macro equivalents. In the macro case, efficiency is almost exclusively measured by the *specific impulse* of the thruster,

$$I_{\text{sp}} = \frac{F_t}{\dot{m} g_0} \tag{4.1}$$

where F_t is the thrust, $\dot{m}$ the mass flow, and g_0 the standard gravity. While the unit of seconds is not the most intuitive, it is easily comparable – more is better. What is notably left out of equation 4.1 is any power consumption. While of little concern for large spacecrafts where the power needed to initiate the combustion of their reactive propellants is negligible compare to their overall power budget, that budget calculation is different for nano satellites. This is why another figure of merit, with the less specific name of *overall thrust efficiency*, η, is important to include when comparing microthrusters. It is defined as

$$\eta = \frac{F_t^2}{2\dot{m}P} = \frac{F_t I_{\text{sp}} g_0}{2P} \tag{4.2}$$

where P is the supplied power. With these two measurements of efficiency, thrusters can be evaluated for the specific use case of miniaturized satellite propulsion.

4.1 Plasma heated cold gas microthrusters

One way to improve the efficiency of cold gas microthrusters is to heat the gas before it gets expelled. In **Paper I** we therefore compare three different ways of heating the gas in a conventional cold gas microthruster design and evaluate both their I_{sp} and overall thrust efficiency. The three heaters were all included

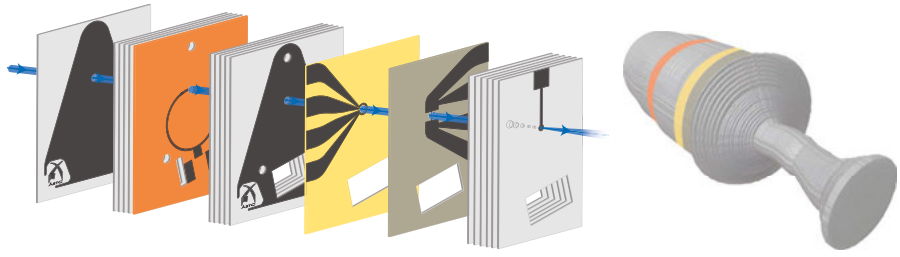

Figure 4.2. Exploded view of the device, with gas flow highlighted in blue and color coded heater sheets: orange for the SSRR, yellow for the screen printed in-plane resistive heater, and dark grey for the platinum wire. On the right is a reconstruction of the stagnation chamber and nozzle based on microCT scans, also color coded to indicate the positions of the heaters.

on the same device, as seen to the left in figure 4.2, one SSRR, one resistive heater screen-printed on the inner wall of the thruster, and one freely suspended platinum wire resistive heater. The latter two could also, independently be used as thermometers when they were not in use as heaters, thus providing information about the amount of power lost to heating the substrate rather than the gas. With ambient temperatures that can dip to below -70 °C heat losses to the substrate is not only a concern from an efficiency stand point, but can also have serious effects on the substrate itself. For this reason, the SSRR with it's ability to selectively heat the gas it ionizes rather than its surrounding was expected to, and did indeed, perform better than the resistive heaters. At a power input to the heaters of 1.1 W, the increase in I_{sp} by the heated gas was two and fifteen times higher for the SSRR than for the wire and in-plane resistive ones, respectively. This corresponded to an overall thrust efficiency of 55% for the SSRR, and 18% and 14% for the wire and in-plane ones.

This type of comparison is of course subject to a number of design choices. The inclusion of all heaters on the same device ensured that they shared a baseline I_{sp} and that the geometry of the stagnation chamber and nozzle was the same. However, it also meant that the design was not optimized for any of the heaters, making it hard to determine how the performance measured in this study would translate to a new design focused on one single heater principle. Additionally, while the comparisons were performed at the same power *delivery*, this does not, necessarily, translate to the same power *draw* for each heater – but without a surrounding system to integrate them into, it is hard to argue for another value to be used.

These are some of the considerations that make the design-build-test-loops for space missions long and costly. To the point made in the beginning of the previous chapter, every single component must be evaluated not just on its own, but as a part of a system that will operate in an environment which is extremely hard to replicate here on Earth.

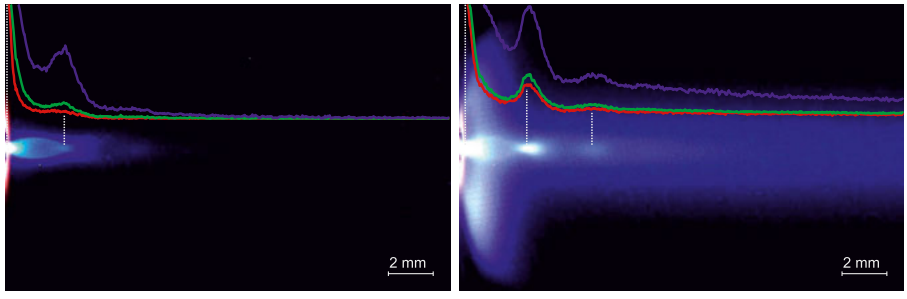

Figure 4.3. Shock cell distances determined by clustered color channel intensity along the exhaust plume centerline for low (left) and high (right) power plasmas.

4.1.1 Plasma properties and thruster efficiency

Looking at equation 4.1 again, measuring the I_{sp} may seem like a straight forward process. The $\dot{m}$ can easily be monitored using a calibrated mass flow sensor, and for F_t all that should be needed is a sufficiently sensitive load cell (weight sensor). The latter, however, often require non-trivial setups with a sensor that offers high resolution, < 0.1 mN, at high loads, > 10 N, and at least a moderate sampling frequency, > 10 Hz. Moreover, as the force generated by almost any type of thruster is dependent on the ambient pressure, measurements are in general performed with the thruster mounted inside a vacuum chamber, putting further demands on the measurement setup. In an effort to circumvent some of these challenges, we estimated the thrust in **Paper I** based on shock cell geometry, see figure 4.3. This was possible as the exhaust of the thruster became visible due to the emissions from the plasma and we could thus exploit the fact that the distance between the nozzle exit and the first shock cell $x \propto p_A/p_1 \propto v_E \approx F_t \dot{m}^{-1}$ [58], where p_A and p_1 are the ambient and stagnation chamber pressures, respectively, and v_E the gas exhaust speed. These estimates were found to be highly correlated with the scale based measurements and thus offers a path to faster iterations in future design optimization.

In the following publication, **Paper II**, the relation between specific plasma properties, such as emission spectroscopy determined ion density and electron temperature (as measured by langmuir probes), and both plasma power and thrust were investigated. The result showed that while certain ionization processes have a higher level of correlation with thrust performance than others, the shock cell geometry approach offers a better thrust estimate in general investigations.

5. Concluding Remarks and Future Work

Now that we have gone from the smallest of incubators to the vastness of space, hammered the fundamentals and analyzed the applied, what is left? A lot, of course! The regression analysis in chapter 2 showed that the modern statistical approaches have the potential to significantly improve applied spectral analysis. It feels a bit ironic, that what I think might be the most important future work in this area – arguably the most fundamental research presented here – is very much applied; making these new methods available in more applied fields, i.e., making them *usable*. Because in the competition of adaptation in the engineering sciences, a shiny new machine learning method is not facing off with next week's state-of-art, it is competing with an old, Fortran-based, rock-solid, long-forgotten, 16-bit windows executable. But as long as the former does not run on a 2000-era, windows 7 workstation it is dead on arrival. So the ironic part then, is that what I hope to see in the future is work on implementing existing methods in software packages that can be run on a wide variety of platforms. And by that I do not mean in web browsers.

The differential gas sensor in **Paper VII** shows great promise, even in what must be described as its most basic form. A significant portion of the work in the study was focused on demonstrating the basic function of the dual, out-of-phase SSRRR system. Therefore there was little time allotted to iterate the design of the setup, something I am sure could bring improvements to the results presented here and in the paper.

On the system side of things, I think the path forward is also quite clear. The future of the TBM-system we presented in papers **III**, **IV**, and **VI** most certainly entails further studies, and hopefully trials involving other people than the authors. The patch design, in its current incarnation shows good performance, but more extensive investigations on the effects and mitigations of both sweat and particle blockages of the fluidics separating the sensor and the patient is needed. The electrical interface and fabrication method introduced in **Paper IV** merely opened the door to further development. As PDMS is extensively used in the rapidly expanding field of wearable medical sensors [59], it seems unlikely that there will be a need to focus much on the development of compatible sensors, but rather on the integration of them.

Finally then, while the ÅSTC has slimmed down in terms of number of active researchers as of late, improvements on the microthruster design presented in **Paper I** has already been published [60] – and further cutting edge research on the materials and fabrication techniques used in space exploration is on the way. Ceramic 3D-printing is soon likely to offer previously unattainably fast

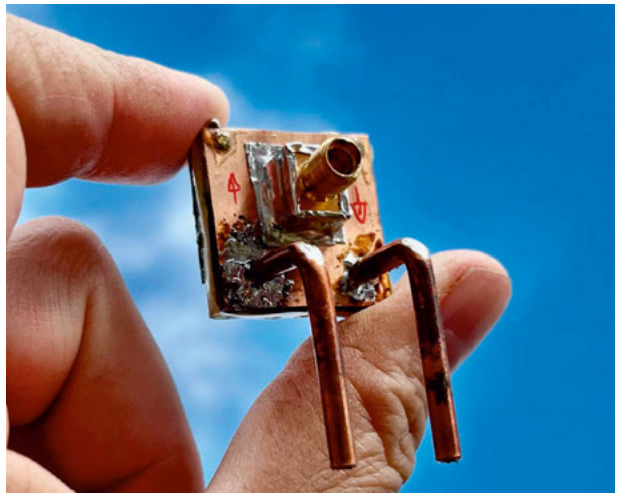

Figure 5.1. A microplasma source very similar to the one that my supervisor gave me on one of my first days, which was only meant to walk me through the different parts of it. It has since then lived on my desk, been lovingly named *the space snail* by my wife, and has been shown off in several seminars and talks. Neither it nor the depicted one is the prettiest of plasmasources, and has not actually produced any plasma in my care, but I liked it. Not enough to not lose it, but enough to have a very similar one be the last picture I add to this thesis.

prototyping-cycles of thruster designs, paving the road for further optimization of cold gas thruster performance. So with a little luck and a lot of prototypes, maybe our little plasma source will soon be able to send its ions right back out into the space that inspired its design in the first place.

6. Acknowledgements

First off, **Anders Persson**, my main supervisor, the guy who had to put with me for a good half a decade. Well, we did take a breather there for a year and had kids (not with each other, but in close temporal proximity). You really were a great supervisor, thank you. That's not to say that the other ones did not contribute; I really appreciated the scientific rigor of **Greger Thornell**, the lessons and help with everything from evaporation deposition to writing in Persian of **Zahra Atena Khaji**, and aside from all the great advice and discussions also the unmatched fika organizing skills of **Klas Hjort** – all of whom, in the order given, were my co-supervisors.

Then there are all my current (at least as of writing) and former colleagues who's help has saved my butt more than once. To properly write out all the fun and helpful things you have been the source of would make this book thicker than a complete MST fabrication manual, so here is an woefully incomplete list of stubs. **Erika Åkerfeldt** my ÅSTC lab buddy, **Peter Sturesson** with all the rocket and Västerbottnian stuff, **Javier Cruz** with the PDMS and the smile, **Federico Cantoni** and the charm, the concrete and the bread, **Ana-Maria Porras Hernández** with the keeping me and all the other ducks in a row, **Abdul Raouf Atif** my desk buddy, **Simon Södergren** is just pleasant to be around, as is **Karolina Svensson**, **Sarah-Sophia Carter** the volleyball and good vibes pro, **Jan Maslik** and **Oskar Hellman** with all the PDMS expertise and letting me borrow all the stuff all the time, **Klara Björnander Rahimi** the original PDMS and chemilab oracle, **Lena Klintberg** bringing the green fingers to the clean room, and **Martin Berglund** the creator of electronics and plasma.

I want to thank my friends who have helped and supported me throughout these years, **Sean Searle** my friend that feeds, **Edvin Norén** who brings the music and *very* high numbers, **Petter Lundberg** who is always there (also, thanks for the intro buddy), my soon to be boat buddies **Igor Tominec** and **Eva Breznik**. On top of that there are the whole host of good people at UmU, and friends in Kiruna, and the wonderful people defending and fighting for our rights as employees at the union in Uppsala and every where else. And, of course, my extended family in Austria and Los Angeles.

Then we have the people that raised me, put up with my rants and ramblings, and so much more. My parents, **Robert** and **Jenny**, and my siblings, **Camilla**, **Sara**, **Lisa**, **Arvid**, **Signe**, and **Rebecka**. You are truly the best ones I could ever imagine. I wish I could tell you all how amazing you have been, and still are. The support, inspiration, and food you provide seem endless and is always fantastic. As are, of course, my bonus siblings, **Anneli**, **Raúl** and **Fredrik**.

And then finally, **Elisabeth**. I love you. Without you I would not even have made it to the starting line, much less the finishing one. I can not thank you enough for the support – academic, emotional, and just practical one. You made this fun and I am so looking forward to keep doing the next thing, and all the ones after that with you.

Last, and more than anything, **Eíra**. There is nothing in the world like playing with you, or listening to you talk. You are the most important and lovely thing in my life, I love you.

7. Svensk sammanfattning

”Varde ljus!” och det blev plasma är inte riktigt det grundlöst populära citatet som många av oss läste i religionskunskapen. Det har nog främst med den dogmatiska oviljan att uppdatera dessa texter allt eftersom vi lär oss mer om jorden, naturen, och rymden. För det är just massiva kroppar av plasma som bestrålar oss med det ljus som vi behöver för att leva. Ett ljus som, förutom att skänka liv, även bär med sig kunskap – det berättar historien om universum, dess bildande, och innehåll.

Som kanske framgår av sammanhanget använder jag *berättar* ganska fritt här. Vanliga konversationer skulle vara förhållandevis påfrestande om det krävdes en hel uppsättning spektrometrar och statistik analys för att kunna tyda vad den andra parten säger. Poängen är att det är möjligt att ta reda på sammansättningen av ohyggligt avlägsen materia utifrån det ljus den ger ifrån sig. Samma princip fungerar dessutom lika bra här på jorden. Här är dock plasma inte lika vanligt – vi träffar på det i norrsken, blixtar, eld, och lustiga lampor – men det är sällan något som vi tänker på som användbart i vardagen, och än mindre som ett verktyg för att skapa mer tillgänglig och bättre medicinsk utrustning. Innan vi går in på hur och varför ett litet plasma kan fylla just en sådan funktion kan det vara värt att förtydliga vad det är.

Plasma uppstår när tillräckligt mycket energi tillförs till en gas för att jonisera gaspartiklarna, d.v.s. få dem att ge ifrån sig en eller fler elektroner som därefter svävar fritt. När tillräckligt många partiklar har joniserats förändras gasens egenskaper till en grad som gör att det inte längre kan kallas gas, utan plasma. Det finns så klart mycket mer att säga om plasma men givet syftet med den här sammanfattningen kan vi nöja oss så och förhålla oss till den mikroplasmakällan som använts i våra studier som en elektronisk komponent som genom att variera spänningen på vardera sida om ett litet hålrum tillför så mycket energi till gasen som befinner sig där att den övergår till plasma.

Studierna som jag tillsammans med mina medförfattare har utfört har gjorts vid Avdelningen för Mikrosystemteknik och Ångström Rymdtekniskt Centre (ÅSTC). Mikrosystem är system vars delar är i storleksordningen av mikrometer, µm, alltså en miljondels meter. För er som kommer ihåg kassettband så är tjockleken på själva banden några µm, en annan referenspunkt är trådarna i fin spindelväv som är av samma tjocklek. En partikel vars storlek inte är mer än några µm åt något håll kan inte ses med blotta ögat – för att det ska vara möjligt krävs närmare 100 µm.

Det är vanligt att dela upp mikrosystemteknik i tre kategorier, *(i)* aktuatorer – komponenter som utför arbete, *(ii)* sensorer – komponenter som reagerar på

stimuli genom att producera någon form av signal, och *(iii)* system – en sammansättning av komponenter som utför en mer komplex uppgift definierad av en tillämpning. Studierna som ligger till grund för denna avhandlingen behandlar alla tre kategorier, där den röda tråden är en specifik komponent – mikroplasmakällan.

I de två första studierna utvärderades mikroplasmakällan som en aktuator, närmare bestämt som en gasvärmare i en mikroraket avsedd för manövrering av små satelliter. En mikroraket fungerar i sin mest grundläggande form som en oknuten ballong som släpps: trycksatt gas far åt ett håll och dragkraften som uppstår skickar satelliten åt det andra. Eftersom det än så länge helt saknas tankstationer i rymden behöver dessa raketer vara bränslesnåla. I den första studien kunde vi konstatera att plasmakällan effektiviserar bränsleanvändningen betydligt mer än konventionella resistiva värmare. Därutöver kunde vi presentera ett nytt sätt att uppskatta effektiviteten hos den plasmavärmda raketen genom att bara titta på dess plym (utblås). I den andra studien, som fokuserade helt på analys av plasmaegenskaperna, upptäcktes korrelationer mellan tillförd effekt, jondensitet, och effektivitet.

Därefter följde en studie av hur plasmakällan kunde användas tillsammans med en spektrometer för att skapa en gassensor. Genom att med spektrometern fånga in det ljusspektrum som plasman emitterade (gav ifrån sig) när en gasblandning med känd sammansättning flödades igenom det kunde vi utvärdera tre olika typer av statistiska regressionsmetoder. Regressionsmetoder används för att ta fram en funktion för, eller approximativ modell av, hur observationer av en sak kan prediktera (förutsäga) en annan. I vårt fall var observationerna ljusspektrum och det vi ville förutsäga var koncentrationen av en viss gas i blandningen. Resultaten av studien visade att det spelar stor roll vilken typ av regressionsmetod man använder när man utför den här typen av analys och att uppställningen med mikroplasmakällan och spektrometern fyllde den avsedda sensorfunktionen väl. En stor fördel med uppställningen var att det breda ljusspektrat kunde avslöja koncentrationen av många olika typer av gaser, men mätningens precision hade viss förbättringspotential. Därför förändrade vi experimentuppställning till nästa studie för att kunna mäta koncentrationen av en specifik gas med hög precision. I den nya uppställningen användes två plasmakällor tillsammans med ett optiskt filter och en fotodiod. Till skillnad från en spektrometer som mäter intensiteten hos varje våglängd (färg) i ljuset, mäter en fotodiod intensiteten hos allt ljus som faller på den samtidigt. Genom att täcka dioden med ett optiskt filter som bara släpper igenom en viss våglängd kunde intensiteten hos just den våglängden mätas med hög precision och studien visade också att med den nya uppställningen kunde användas som en differentiell gasanalysator.

I de tre avslutande studierna integrerades gassensorn i ett system för transkutan (hudgenomträngande) blodgasövervakning, eller transuctaneous blood gas monitoring (TBM) på engelska. TBM-utrustning används för att icke-invasivt (utan fysisk åverkan, i det här fallet utan att sticka hål på

huden) mäta halten koldioxid och syre i blodet på en patient. Metoden används framförallt på intensivvårdsavdelningar för barn, i huvudsak på prematurt (för tidigt) födda. Liksom de flesta medicinska åkommor drabbar effekterna av prematur födsel människor som bor i delar av världen som lider av de ekonomiska sviterna av kolonisering, förslavning, och krig, värst. Ett, enligt WHO, extremt prematurt barn (fött tidigare än vecka 28) som föds i ett höginkomstland löper runt 10% risk att dö. Motsvarande siffra i utvecklingsländer är över 90%. En stark motivation för dessa studier var därför att skapa ett modulärt system där förbrukningsdelarna skulle kunna tillverkas billigt och vid behov utan tillgång till högteknologisk utrustning.
Befintliga TBM-system bygger på en teknik där gasen som tränger ut genom huden diffunderar in i en uppvärmd sensor tillverkad av hårdplast. Tekniken är långsam, det tar ofta många minuter från att sensorn har satts fast på en patient tills dess en användbar signal visas, och den måste flyttas ofta. I den första studien utvecklade vi därför en passiv, mjuk gasinsamlare som via ett tunt, flexibelt rör transporterade gasen från huden till mikroplasmasensorn. Gasinsamlaren kan tillverkas helt utan avancerad utrustning utifrån en mall av kiselgummi. Den påföljande studien syftade till att utveckla en enkel och skalbar tillverkningsmetod för att integrera värmare och andra elektriska komponenter i gasinsamlaren. Med tillverkningsmetoden kunde vi bygga en värmarprototyp som kunde leverera en initial värmepuls genom gasinsamlaren mer än 10 gånger mer effektivt än en vanlig resistiv värmare. I den sista studien presenterades TBM-systemet i sin helhet tillsammans med en teoretisk modell för hur koldioxiden som förs in i sensorn relaterar till koldioxidhalten i blodet.

Avslutningsvis så tror jag kanske inte att den här avhandlingen kommer ligga till grund för några nya revisioner av religiösa texter, men förhoppningsvis så har den bidragit till att de approximativa modeller vi har av universum blivit lite bättre. För oss som nu föredrar det över dogmer.

Bibliography

[1] Marc J. Madou. *Fundamentals of Microfabrication and Nanotechnology, Three-Volume Set*. Taylor & Francis, Andover, England, UK, 2011.

[2] Jérôme Charmet, Rui Rodrigues, Ender Yildirim, Pavan Kumar Challa, Benjamin Roberts, Robert Dallmann, and Yudan Whulanza. Low-Cost Microfabrication Tool Box. *Micromachines*, 11(2):135, January 2020.

[3] Nathan Zavanelli and Woon-Hong Yeo. Advances in Screen Printing of Conductive Nanomaterials for Stretchable Electronics. *ACS Omega*, 6(14):9344–9351, April 2021.

[4] M. A. Câmara, J. C. Campos Rubio, A. M. Abrão, and J. P. Davim. State of the Art on Micromilling of Materials, a Review. *Journal of Materials Science & Technology*, 28(8):673–685, August 2012.

[5] Rutvik Lathia, Krishnadas Narayanan Nampoothiri, Nitish Sagar, Shubhi Bansal, Chandantaru Dey Modak, and Prosenjit Sen. Advances in Microscale Droplet Generation and Manipulation. *Langmuir*, 39(7):2461–2482, February 2023.

[6] M. Berglund, M. Gruden, G. Thornell, and A. Persson. Evaluation of a microplasma source based on a stripline split-ring resonator. 22(5):055017. Publisher: IOP Publishing.

[7] Martin Berglund. *Miniature Plasma Sources for High-Precision Molecular Spectroscopy in Planetary Exploration*. PhD thesis, Acta Universitatis Upsaliensis, 2015.

[8] Anders Persson, Martin Berglund, Greger Thornell, Göran Possnert, and Mehran Salehpour. Stripline split-ring resonator with integrated optogalvanic sample cell. *Laser Physics Letters*, 11(4):045701, February 2014.

[9] Helmut Gernsheim. *A concise history of photographs*. Dover photography collections. Dover Publications, Mineola, NY, 3 edition, May 1987.

[10] Woo-Tae Kim, Cheonwi Park, Hyunkeun Lee, Ilseop Lee, and Byung-Geun Lee. A High Full Well Capacity CMOS Image Sensor for Space Applications. *Sensors*, 19(7):1505, March 2019.

[11] T. D. Wang, C. L. Liu, and N. M. Liao. Development of a High-Frame-Rate CCD for Lightning Mapping Imager on FY-4. In *5th International Symposium of Space Optical Instruments and Applications*, pages 287–293. Springer, Cham, Switzerland, January 2020.

[12] Derek M. Kita, Brando Miranda, David Favela, David Bono, Jerome Michon, Hongtao Lin, Tian Gu, and Juejun Hu. High-performance and scalable on-chip digital fourier transform spectroscopy. 9(1):4405.

[13] Shima Nezhadbadeh, A. Neumann, Payman Zarkesh-Ha, and S. R. J. Brueck. Chirped-grating spectrometer-on-a-chip. *Opt. Express*, 28(17):24501–24510, Aug 2020.

[14] Hans Griem. *Spectral Line Broadening by Plasmas*. Academic Press, Cambridge, MA, USA, January 1974.

[15] Fred C. Adams and Gregory Laughlin. A dying universe: the long-term fate and evolutionof astrophysical objects. *Rev. Mod. Phys.*, 69:337–372, Apr 1997.
[16] R. Bellman, Rand Corporation, and Karreman Mathematics Research Collection. *Dynamic Programming*. Rand Corporation research study. Princeton University Press, 1957.
[17] Stefan Rännar, Fredrik Lindgren, Paul Geladi, and Svante Wold. A PLS kernel algorithm for data sets with many variables and fewer objects. Part 1: Theory and algorithm. *Journal of Chemometrics*, 8(2):111–125, March 1994.
[18] Leo Breiman. Bagging predictors. *Machine Learning*, 24(2):123–140.
[19] George E. P. Box. Science and Statistics. *Journal of the American Statistical Association*, 71(356):791–799, December 1976.
[20] Peter R Griffiths and James A De Haseth. *Fourier transform infrared spectrometry*, volume 171. John Wiley & Sons, 2 edition, 2007.
[21] Roman Rosipal and Nicole Krämer. Overview and Recent Advances in Partial Least Squares. In *Subspace, Latent Structure and Feature Selection*, pages 34–51. Springer, Berlin, Germany, 2006.
[22] S. Wold, A. Ruhe, H. Wold, and Iii Dunn, W. J. The collinearity problem in linear regression. the partial least squares (PLS) approach to generalized inverses. *SIAM Journal on Scientific and Statistical Computing*, 5(3):735–743. Publisher: Society for Industrial and Applied Mathematics.
[23] Roman Rosipal. *Nonlinear Partial Least Squares: An Overview*. January 2010.
[24] Ildiko E. Frank. A nonlinear PLS model. *Chemometrics and Intelligent Laboratory Systems*, 8(2):109–119, June 1990.
[25] Svante Wold, Nouna Kettaneh-Wold, and Bert Skagerberg. Nonlinear PLS modeling. *Chemometrics and Intelligent Laboratory Systems*, 7(1):53–65, December 1989.
[26] Roman Rosipal and Leonard J. Trejo. Kernel partial least squares regression in reproducing kernel hilbert space. *The Journal of Machine Learning Research*, 2:97–123.
[27] Trevor Hastie, Robert Tibshirani, and J. H. Friedman. *The elements of statistical learning: data mining, inference, and prediction*. Springer series in statistics. Springer, 2nd ed edition.
[28] Hervé Abdi. Partial least squares regression and projection on latent structure regression (PLS Regression). *WIREs Computational Statistics*, 2(1):97–106, January 2010.
[29] Diederik P. Kingma and Jimmy Ba. Adam: A method for stochastic optimization. *arXiv:1412.6980 [cs]*.
[30] Åsmund Rinnan, Frans van den Berg, and Søren Balling Engelsen. Review of the most common pre-processing techniques for near-infrared spectra. 28(10):1201–1222.
[31] Tarald O. Kvalseth. Cautionary note about r 2. 39(4):279.
[32] ISO. Accuracy (trueness and precision) of measurement methods and results – Part 1: General principles and definitions.
[33] Hannah Blencowe, Simon Cousens, Mikkel Z. Oestergaard, Doris Chou, Ann-Beth Moller, Rajesh Narwal, Alma Adler, Claudia Vera Garcia, Sarah Rohde, Lale Say, and Joy E. Lawn. National, regional, and worldwide estimates of preterm birth rates in the year 2010 with time trends since 1990 for selected

countries: a systematic analysis and implications. *Lancet*, 379(9832):2162–2172, June 2012.
[34] Jamie Perin, Amy Mulick, Diana Yeung, Francisco Villavicencio, Gerard Lopez, Kathleen L. Strong, David Prieto-Merino, Simon Cousens, Robert E. Black, and Li Liu. Global, regional, and national causes of under-5 mortality in 2000–19: an updated systematic analysis with implications for the Sustainable Development Goals. *Lancet Child & Adolescent Health*, 6(2):106–115, February 2022.
[35] James C. Lin, Ronald G. Strauss, Jeff C. Kulhavy, Karen J. Johnson, M. Bridget Zimmerman, Gretchen A. Cress, Natalie W. Connolly, and John A. Widness. Phlebotomy Overdraw in the Neonatal Intensive Care Nursery. *Pediatrics*, 106(2):e19, August 2000.
[36] J. W. Severinghaus. Methods of measurement of blood and gas carbon dioxide during anesthesia. *Anesthesiology*, 21:717–26, November 1960.
[37] P. Eberhard and R. Schäfer. A Sensor For Non Invasive Monitoring of Carbon Dioxide. *Journal of Clinical Engineering*, 6(1):35, January 1981.
[38] Ian Bromley. Transcutaneous monitoring–understanding the principles. *Infant*, 4(3):95–98, 2008.
[39] World Health Organization et al. Core medical equipment. Technical report, World Health Organization, 2011.
[40] Peter Hoeger, Veronica Kinsler, Albert Yan, John Harper, Arnold Oranje, Christine Bodemer, Margarita Larralde, David Luk, Vibhu Mendiratta, and Diana Purvis. *Harper's Textbook of Pediatric Dermatology*. November 2019.
[41] Valerie Miké, Alfred N. Krauss, and Gail S. Ross. Doctors and the health industry: A case study of transcutaneous oxygen monitoring in neonatal intensive care. *Social Science & Medicine*, 42(9):1247–1258, May 1996.
[42] Hajime Matsumura, Ryutaro Imai, Niyaz Ahmatjan, Yukiko Ida, Masahide Gondo, Dai Shibata, and Katsueki Wanatabe. Removal of adhesive wound dressing and its effects on the stratum corneum of the skin: comparison of eight different adhesive wound dressings. *International Wound Journal*, 11(1):50–54, February 2014.
[43] C. Liu. Recent Developments in Polymer MEMS. *Advanced Materials*, 19(22):3783–3790, November 2007.
[44] V. A. Harpin and N. Rutter. Sweating in preterm babies. *Journal of Pediatrics*, 100(4):614–619, April 1982.
[45] W. Magerl and R. D. Treede. Heat-evoked vasodilatation in human hairy skin: axon reflexes due to low-level activity of nociceptive afferents. *Journal of Physiology*, 497(3):837–848, December 1996.
[46] Alberto Piqué, Scott A. Mathews, Nicholas A. Charipar, and Andrew J. Birnbaum. Laser origami: a new technique for assembling 3D microstructures. In *Proceedings Volume 8244, Laser-based Micro- and Nanopackaging and Assembly VI*, volume 8244, pages 72–78. SPIE, February 2012.
[47] Adam L. Bachmann, Brendan Hanrahan, Michael D. Dickey, and Nathan Lazarus. Self-Folding PCB Kirigami: Rapid Prototyping of 3D Electronics via Laser Cutting and Forming. *ACS Appl. Mater. Interfaces*, 14(12):14774–14782, March 2022.
[48] Bendong Liu, Xinrui Li, Jiahui Yang, and Guohua Gao. Recent Advances in

MEMS-Based Microthrusters. *Micromachines*, 10(12):818, November 2019.
[49] Carole Rossi, Daniel Estève, and Corinne Mingués. Pyrotechnic actuator: a new generation of Si integrated actuator. *Sensors and Actuators A: Physical*, 74(1):211–215, April 1999.
[50] Xue Yan, Chang Jun Shi, Ren Xiaoming, Liu Lan, and Rui Zhen Xie. Study of MEMS Based Micropyrotechnic Igniter. *Applied Mechanics and Materials*, 472:750–755, 2014.
[51] E. V. Mukerjee, A. P. Wallace, K. Y. Yan, D. W. Howard, R. L. Smith, and S. D. Collins. Vaporizing liquid microthruster. *Sensors and Actuators A: Physical*, 83(1):231–236, May 2000.
[52] X. Wang, Z. Fei, V. L. Wong, Y. Ren, and K. H. Cheah. Additively manufactured vaporizing liquid microthruster with micro pin fins for enhanced heat transfer. *Acta Astronautica*, 199:58–70, 2023.
[53] Salvo Marcuccio, Angelo Genovese, and Mariano Andrenucci. Experimental Performance of Field Emission Microthrusters. *Journal of Propulsion and Power*, 14(5):774–781, September 1998.
[54] Lars Stenmark, Ylva Bäcklund, Johan Köhler, K. Larsson, and Urban Simu. Micro propulsion thrusters for space applications. 3rd Micro Structure Workshop, pages 12.1–12.8, Uppsala, 1998.
[55] Johan Köhler, Johan Bejhed, Henrik Kratz, Fredrik Bruhn, Ulf Lindberg, Klas Hjort, and Lars Stenmark. A hybrid cold gas microthruster system for spacecraft. *Sensors and Actuators A: Physical*, 97-98:587–598, April 2002.
[56] Kristoffer Palmer, Ernesto Vargas Catalan, Ville Lekholm, and Greger Thornell. Investigation of exhausts from fabricated silicon micronozzles with rectangular and close to rotationally symmetric cross-sections. *Journal of Micromechanics and Microengineering*, 23(10):105001, August 2013.
[57] C. Rossi. Micropropulsion for Space — A Survey of MEMS-based Micro Thrusters and their Solid Propellant Technology. *Sensors Update*, 10(1):257–292, January 2002.
[58] Ville Lekholm, Kristoffer Palmer, and Greger Thornell. Schlieren imaging of microthruster exhausts for qualitative and quantitative analysis. *Meas. Sci. Technol.*, 23(8):085403, May 2012.
[59] Yingying Yuan, Bo Liu, Hui Li, Mo Li, Yingqiu Song, Runze Wang, Tianlu Wang, and Hangyu Zhang. Flexible Wearable Sensors in Medical Monitoring. *Biosensors*, 12(12):1069, November 2022.
[60] Erika Åkerfeldt, Lena Klintberg, and Greger Thornell. Systematic variation of design aspects for a significant increase in thermal fracture resistance of alumina microthrusters. *J. Micromech. Microeng.*, 31(8):085005, June 2021.
[61] Frank L. Pedrotti, Leno Matthew Pedrotti, and Leno S. Pedrotti. *Introduction to optics*. Pearson/Prentice Hall, 3rd ed edition.
[62] Swaraj Bandhu Mahato, Steven Thijs, Jonas Bentell, Linkun Wu, Klaas Tack, Pierre Boulenc, Dorian Lasnet, Renaud Van Langendonck, and Piet De Moor. Multispectral CCD-in-CMOS time delay integration imager for high resolution earth observation. Publisher: arXiv Version Number: 1.
[63] I.E. Gordon, L.S. Rothman, R.J. Hargreaves, R. Hashemi, E.V. Karlovets, F.M. Skinner, E.K. Conway, C. Hill, R.V. Kochanov, Y. Tan, P. Wcisło, A.A. Finenko, K. Nelson, P.F. Bernath, M. Birk, V. Boudon, A. Campargue, K.V.

Chance, A. Coustenis, B.J. Drouin, J.–M. Flaud, R.R. Gamache, J.T. Hodges, D. Jacquemart, E.J. Mlawer, A.V. Nikitin, V.I. Perevalov, M. Rotger, J. Tennyson, G.C. Toon, H. Tran, V.G. Tyuterev, E.M. Adkins, A. Baker, A. Barbe, E. Canè, A.G. Császár, A. Dudaryonok, O. Egorov, A.J. Fleisher, H. Fleurbaey, A. Foltynowicz, T. Furtenbacher, J.J. Harrison, J.–M. Hartmann, V.–M. Horneman, X. Huang, T. Karman, J. Karns, S. Kassi, I. Kleiner, V. Kofman, F. Kwabia–Tchana, N.N. Lavrentieva, T.J. Lee, D.A. Long, A.A. Lukashevskaya, O.M. Lyulin, V.Yu. Makhnev, W. Matt, S.T. Massie, M. Melosso, S.N. Mikhailenko, D. Mondelain, H.S.P. Müller, O.V. Naumenko, A. Perrin, O.L. Polyansky, E. Raddaoui, P.L. Raston, Z.D. Reed, M. Rey, C. Richard, R. Tóbiás, I. Sadiek, D.W. Schwenke, E. Starikova, K. Sung, F. Tamassia, S.A. Tashkun, J. Vander Auwera, I.A. Vasilenko, A.A. Vigasin, G.L. Villanueva, B. Vispoel, G. Wagner, A. Yachmenev, and S.N. Yurchenko. The HITRAN2020 molecular spectroscopic database. 277:107949.

[64] Alexander Kramida and Yuri Ralchenko. NIST atomic spectra database, NIST standard reference database 78. Type: dataset.

[65] Hannah Ritchie and Max Roser. Technology adoption. *Our World in Data*, 2017. https://ourworldindata.org/technology-adoption.

[66] C. Schierle and M. Otto. Comparison of a neural network with multiple linear regression for quantitative analysis in ICP-atomic emission spectroscopy. 344(4):190–194.

[67] Mohamad KHAYATZADEH Mahani, Marzieh Chaloosi, Mohamad GHANADI Maragheh, Ali Reza Khanchi, and Dariush Afzali. Comparison of artificial neural networks with partial least squares regression for simultaneous determinations by ICP-AES. 25(11):1658–1662.

[68] Husheng Yang, Peter R. Griffiths, and J. D. Tate. Comparison of partial least squares regression and multi-layer neural networks for quantification of nonlinear systems and application to gas phase fourier transform infrared spectra. 489(2):125–136.

[69] Sijmen de Jong. SIMPLS: An alternative approach to partial least squares regression. *Chemometrics and Intelligent Laboratory Systems*, 18(3):251–263.

[70] Niels Asger Mortensen, Fridolin Okkels, and Henrik Bruus. Reexamination of Hagen-Poiseuille flow: Shape dependence of the hydraulic resistance in microchannels. *Physical Review E*, 71(5):057301, May 2005.

[71] Wiley J Larson, James Richard Wertz, et al. *Space Mission Analysis and Design*, volume 3. Springer, 1992.

Acta Universitatis Upsaliensis

Digital Comprehensive Summaries of Uppsala Dissertations from the Faculty of Science and Technology 2272

Editor: The Dean of the Faculty of Science and Technology

A doctoral dissertation from the Faculty of Science and Technology, Uppsala University, is usually a summary of a number of papers. A few copies of the complete dissertation are kept at major Swedish research libraries, while the summary alone is distributed internationally through the series Digital Comprehensive Summaries of Uppsala Dissertations from the Faculty of Science and Technology. (Prior to January, 2005, the series was published under the title "Comprehensive Summaries of Uppsala Dissertations from the Faculty of Science and Technology".)

Distribution: publications.uu.se
urn:nbn:se:uu:diva-500778

ACTA UNIVERSITATIS
UPSALIENSIS
2023